Horizon 2020
European Union Funding
for Research & Innovation

GEARBODIES

Grant Agreement Number: 101013296
Project Acronym: GEARBODIES
Project title: Innovative Technologies for Inspecting Carbodies and for Development of Running Gear

DELIVERABLE D 4.2
Modelling of rail vehicle dynamics and simulation of running gear loads

Project acronym:	GEARBODIES
Starting date:	01/12/2020
Duration (in months):	25
Call (part) identifier:	H2020-S2R-OC-IP1-02-2020
Grant agreement no:	101013296
Grant Amendments:	N/A
Due date of deliverable:	30-06-2021
Actual submission date:	22-11-2021
Coordinator:	Patrick Schneider
Lead Beneficiary:	RWTH
Version:	1.0
Type:	Report
Sensitivity or Dissemination level:	Public
Contribution to S2R TDs or WAs	TD1.4 running gear
Taxonomy/keywords:	journal, axlebox, bearing, elastomeric suspension; trailing arm bushing; specifications; multibody simulations; highspeed vehicle;

This project has received funding from the Shift2Rail Joint Undertaking (JU) under grant agreement 101013296. The JU receives support from the European Union's Horizon 2020 research and innovation programme and the Shift2Rail JU members other than the Union.

Document history

Revision	Date	Description
0.1	19/05/2021	RWTH structure of deliverable
0.2	24/08/2021	RWTH change of structure, adding §3,§4,§5.1-2,§6.1
0.3	01/09/2021	RWTH start with §3.2
0.4	15/10/2021	UNEW §4,$5.3,$6.2, DICEA comments and §1,§2
0.5	17/10/2021	DICEA executive summary, RWTH $7,
0.6	19/10/2021	DICEA and RWTH improvement of §4,UNEW improvement of §6.2,RWTH improvement on §6.1, VGTU §3.2
0.7	29/10/2021	RWTH restructuring §6
0.8	05/11/2021	Review by Riccardo LICCIARDELLO (DICEA), adjustment by RWTH
1.0	08/11/2021	RWTH last formatting
1.0	19/11/2021	Final review

Report contributors

Name	Beneficiary Short Name	Details of contribution
Iman HAZRATI	UNEW	§4,§5.3,§6.2
Sina SHAHIDZADEH ARABANI	DICEA	§5.2,§6.1
Patrick SCHNEIDER	RWTH	§1,§2,§3.1,§4,$5.1,§5.2,§6.1,§7
Riccardo LICCIARDELLO	DICEA	Executive Summary,§2,§7
Gintautas BUREIKA	VGTU	§3.2
Celestino SÁNCHEZ	EUR	Final review

Disclaimer

The information in this document is provided "as is", and no guarantee or warranty is given that the information is fit for any particular purpose. The content of this document reflects only the author's view – the Shift2Rail Joint Undertaking is not responsible for any use that may be made of the information it contains. The users use the information at their sole risk and liability.

Table of contents

List of figures

List of tables

Executive Summary

The purpose of this report is to provide a reference case for running gear loads through Multi-Body Simulation (MBS) of a virtual reference vehicle on a virtual reference track. The loads determined with this activity are considered as a benchmark against which the loads of an upgraded vehicle model to be developed in future work of WP7 will be compared. The upgraded model will comprise the GEARBODIES innovations regarding elastomeric components and journal bearings, so as to examine the differences with the reference case.

The core part of the report starts with a description of the relevant information from the standards that describe the test cycles for elastomeric components and journal bearings. This is because the focus of GEARBODIES work is the lifetime of these components, and the test cycles are intended to be representative of the loads encountered during the lifetime. In the results section, the MBS benchmark loads are compared with the test cycle loads.

The report then describes the operational scenarios developed for the benchmark case. Such scenarios were based on the "high-speed use case (SPD1)" developed in previous SHIFT2RAIL projects, particularly IMPACT-1. The IMPACT-1 track is approximately 300 km long. In order to maintain the MBS work compatible with the available resources in GEARBODIES, the track is analysed by curve radius and operating velocity to derive simplified GEARBODIES scenarios

The vehicle chosen for the MBS work is a virtual representation of a trailing vehicle of the high-speed ICE-1 trainset of the 1990s. The main criterion for the choice was the availability of public data. Based on the public data, two separate work streams following similar approaches were carried out. The first one investigates the loads on elastomeric components in railway vehicle applications and their consideration in the tests of new components required by the standards. The other one focused on the loads on journal bearings and their current representation in the test cycles.

For the investigation of the loads on elastomeric components the bogie needed to be redesigned. A common design of the primary suspension was implemented, consisting of a trailing arm axle-box connected with an elastomeric bushing to the bogie frame. The corresponding model was then used to simulate the scenarios.

For the investigation of the loads on the journal bearings, the running gear of the base vehicle created some difficulties in the project work. Its secondary suspension is of a design that is no longer common (secondary springs resting on a pendular bolster). Also, the primary suspension, with its longitudinal stiffness provided mainly by a leaf spring, is no longer common. This led to inadequate dynamic behaviour at higher speeds, 300 km/h but also 200 km/h in curves. Significant effort was put into a partial redesign of the running gear to increase its critical speed and reduce the lateral oscillations in curves, the

original ones leading to unrealistically high loads on the bearings and other components. Moreover, its elastomeric components do not (completely) match those identified, in the meantime, through collaboration with PIVOT-2.

The results reported address the loads determined with the refined vehicle model and preliminary considerations on their comparison with the test cycle loads.

In conclusion, a vehicle model and operational scenarios compatible with SPD1 “high speed” are available as a basis for further work. The determined benchmark loads are indicative and useful. They have allowed a better understanding of the relationship between test-cycle loads and expected component lifetime. They provide key indications for the development work in WP5 and WP6. Finally, they are a starting point for the validation activities of WP7.

Abbreviations and acronyms

Abbreviation/ Acronym	Description
DoF	Degrees of Freedom
MBS	Multibody Simulation
PIVOT2	Performance Improvement for Vehicles on Track 2 (S2R IP1 project)
S2R	Shift2Rail Joint Undertaking (under the H2020 framework)
SOA	State-Of-the-Art
SPD	System Platform Demonstrator
TC	Technology Concept
TD1.3	Technology Demonstrator 1.3 within IP1 of S2R (Carbody Shell Demonstrator)
TD1.4	Technology Demonstrator 1.4 within IP1 of S2R (Running Gear Demonstrator)
TRL	Technology Readiness Level
WP	Work Package
WS	Work Stream

1. Introduction

This report represents deliverable 4.2 "Modelling of rail vehicle dynamics and simulation of running gear loads" of the project GEARBODIES, funded by the European Commission within the Shift2Rail (S2R) programme.

As a part of the Innovation Programme 1(IP1) "Cost-efficient and reliable trains, including high-capacity trains and high-speed trains" of S2R, within the framework of Horizon 2020, the project should contribute to two Technology Demonstrators (TD): TD1.3 Carbody Shell and TD1.4 Running Gear.

This deliverable contributes solely to TD1.4. Due to the structure of GEARBODIES, the work on TD1.3 is carried out in a parallel Work Stream. Work Stream 2, including the work package WP4 related to this deliverable, focusses on innovative approaches for developing running gear components.

In WS2 of GEARBODIES the contributing partners aim to develop new elastomeric components and wheelset journal bearings in railway bogies. For both, a TRL of 4-5 is the target.

In the development process, executed in the WP 4-6 of GEARBODIES WS 2, it is necessary to assess the loads the components must endure. Furthermore, for the evaluation of the impact of the component innovations, a benchmark needs to be developed for the further validation work of WP7.

For this purpose, Multi-Body Simulations (MBS) and the related models were developed to assess and evaluate the loads on the components and investigate their representation in the current development and testing process of new components. In the following WP7, the models will be equipped with the components developed in the meantime, so as to investigate their impact on vehicle performance.

Considering this background, the universities contributing to GEARBODIES worked out simulation models and approaches for the given tasks. UNEW and VGTU focussed on the investigation of novel elastomeric components and their behaviour in railway vehicles. DICEA and RWTH investigated the performance of journal bearings.

As a first step in this WP, for both applications, the relevant standards defining the test cycles on the basis of vehicle dynamics considerations, were investigated. Then the operation of high-speed trains is investigated, and simulation scenarios, valid for both components, are developed. Subsequently, a publicly available model of a high-speed train was used and adapted to the respective focus of both work approaches. With the adapted models and the simulation scenarios, the loads on the components were determined.

Limitations to the availability of high-quality high-speed vehicle data resulted in significant efforts to adapt the model so as to achieve satisfactory vehicle dynamics performance. Such efforts generated results and models that are useful and can fulfil their purpose.

2. Objective/Aim

The aim of the work described in this report is to determine the loads acting on the components to be developed in GEARBODIES (i.e. elastomeric components and journal bearings). The loads are determined in scenarios that are both a. useful as a benchmark for the validation activities to be performed in WP7, b. compatible with the overall SHIFT2RAIL action plan for TD1.4. For this purpose, the System Platform Demonstrator SPD1 "high speed" was chosen as a reference. Although in GEARBODIES the elastomeric components within scope cover in principle several different SPDs – differently from journal bearings whose scope is only high-speed applications – SPD1 is considered as a useful focus for both work-streams.

This above aim was translated into specific objectives.

The first objective was to develop MBS models of a high-speed train and simplified scenarios compatible with SPD1 "high speed". The reference train is thus a train for high-speed applications for which the relevant data is available. Based on the availability of data, the choice was the ICE-1 trainset that entered service in the 90s in Germany. The running gear design of the trailer vehicle used as a reference is not ideal, since it is a design no longer in widespread use. In order to maximise the usefulness of this choice, small modifications to the running gear have been made depending on the focus of the investigation without redesigning the whole vehicle. Thereby, two separate adaptations of the vehicle, one with focus on the elastomeric components and one with focus on the journal bearings, were developed.

The second objective was to produce MBS results regarding the loads acting on the elastomeric components and the journal bearings of the ICE-1 in the scenarios compatible with SPD1. This involved "reducing" the SPD1 use case described in (DLR 2018) in the following way. First of all, the given track curvature was assigned to classes and three use cases for the vehicle were put in relation to that. The first described the operation in areas around the station with very narrow curves and low speeds. The second refers to slower parts of the operation in curves leading to a need for reducing speed. Finally, the third scenario represents high-speed operation with high-radius curves and high speed.

Based on the developed models and scenarios, the loads on the components to be developed are investigated. In WP7 later in the project, the scenarios and the models will be used as benchmarks for evaluating the developments.

3. The investigated standards

To evaluate the compatibility of the standard test cycles with the loads simulated for the high-speed use case, an overview of the current processes is given in this chapter. The aim and the methods of the investigated standards are described.

3.1. EN 12082: performance testing of axleboxes

The aim of the investigated standard is to transfer loads resulting from the vehicle dynamics onto the bearing through a suitable test cycle, to guarantee the correct performance of the bearing. Considering that the work package focusses on the vehicle dynamics, the parts of the standards describing or testing for other characteristics or conditions other than mechanical phenomena are neglected in the following description. After the described test cycle, the standard demands operational testing to determine the actual maintenance intervals in detail. The process itself is defined very briefly and will not be described in this deliverable.

3.1.1. The proposed test cycle

For the test cycle of journal bearings in railway applications, three separate parameters need to be determined. The schematic design of a test bench is shown in the following Figure 1.

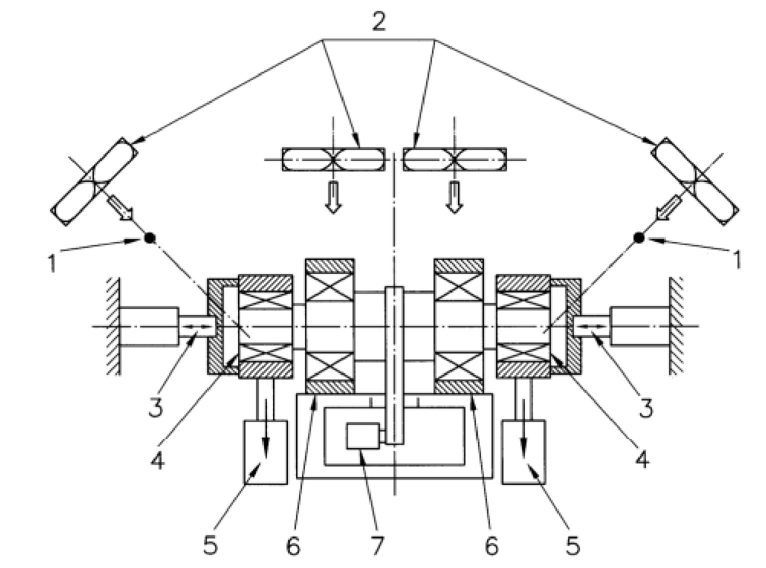

1	Temperature sensor
2	Cooling fans
3	Axial Force, actuator and sensor
4	Bearing to be tested
5	Radial force, actuator and sensor
6	Support bearing
7	Motor

Figure 1: Schematic test bench for bearing tests

The standard defines a test cycle for the radial and axial forces of the bearing to be tested and the number of revolutions per minute. The test process is separated into a pre-test and the actual test for the endurance of the bearing. The pre-test is used to investigate the thermal behaviour of the bearing and to distribute the grease in the bearing before the tests. In the following analysis, this will not be further elaborated.

The defining parameters of the test cycle are set depending on the category of the vehicle the bearings are going to be used in. The listed categories of vehicles are

1. passenger traffic with a maximal operational speed above 200 km/h
2. passenger traffic with a maximal operational speed under or equal to 200 km/h
3. freight traffic
4. urban traffic.

Depending on the vehicle category and its operating velocity, the distance to be tested and the fraction to be run at higher or lower velocity are determined by the standard. This separation for the sequences to be tested is shown in Table 1

Category	Overall track	Fraction at higher velocity	Fraction at lower velocity
$v > 200 \frac{km}{h}$	$8 \cdot 10^5 km$	70	30
$100 \frac{km}{h} < v \leq 200 \frac{km}{h}$ (including Freight and Passenger traffic)	$6 \cdot 10^5 km$	50	50
$v \leq 100 \frac{km}{h}$ (including Freight and Urban traffic)	$4 \cdot 10^5 km$	75	25

Table 1: Fraction of test velocities depending on the operation class

The standard gives an equation for the revolutions per minute to be tested

$$n_{test} = \frac{110 \cdot v_{max}}{6 \cdot \pi \cdot d_{average}}$$

With v_{max} expressed in km/h, and $d_{average}$ in m. $d_{average}$ is the average of the minimum and maximum allowed diameter of the wheels:

$$d_{average} = \frac{d_{min} + d_{max}}{2}$$

A 10% increment of the angular velocity corresponding to maximum speed and average diameter is considered.

The forces acting on the bearing are defined by considering those occurring during the operation of the vehicle with a safety factor. The radial force is determined as 120% of the vertical load per bearing, resulting from the vertical force per wheelset F_0, defined as the vertical force of the whole vehicle divided by the number of wheelsets j.

$$F_0 = \frac{1}{j} \cdot m_{ges} \cdot g$$

From this force F_0 the mass of the wheelset m_2 is subtracted and the force is evenly split between the two bearings of the wheelset. This force is then multiplied with the safety factor 1.2 to consider 120% of the force.

$$F_{rn} = \frac{1.2}{2} \cdot (F_0 - m_2 \cdot g)$$

This radial force is kept constant during the test cycle. How the safety factor was determined is not further elaborated.

The given formula for the determination of the axial force in the standard is not mandatory. Still, it is considered as a reference in this deliverable. For loads in the actual test, the axial force might be concluded from measurements or simulations. If those are not given it should be determined by the following equation:

$$F_{an} = \frac{1.2}{2} \cdot 0.5 \cdot 0.85 \cdot (10^4 + \frac{F_0}{3})$$

From the calculated rotational speed and the axial force, a repeating cycle of increasing, constant and decreasing velocity or force is defined. The rotational velocity is shown in Figure 2 and the axial force in Figure 3. The axial force is applied, while at least 20% of the test bench drives with 20% of the rotational speed. This can be described as the following condition:

$$\frac{n}{n_{test}} \geq 0.2$$

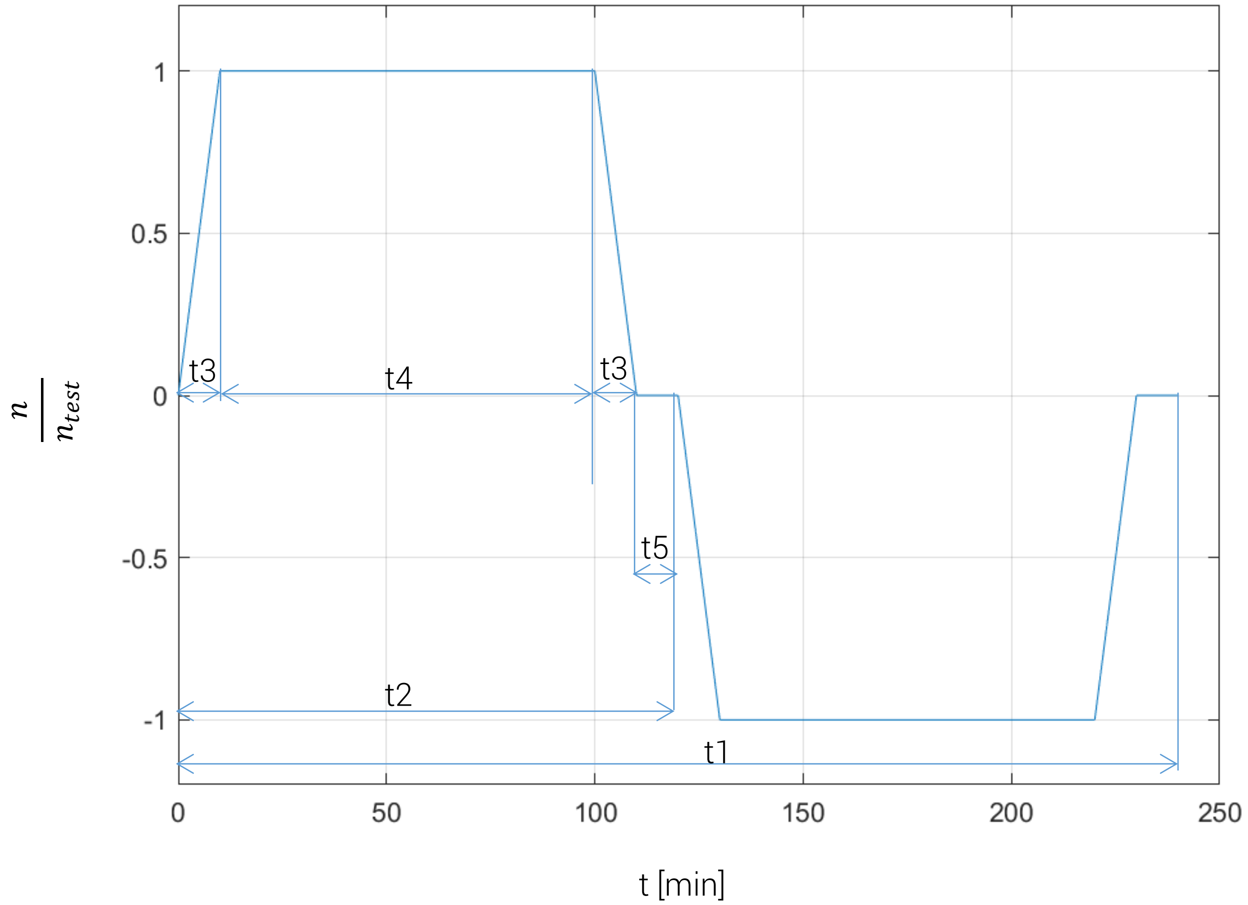

<table>
<tr><th rowspan="2">v_{max}</th><th colspan="5">Time</th></tr>
<tr><th>t1 [min]</th><th>t2 [min]</th><th>t3 [min]</th><th>t4 [min]</th><th>t5 [min]</th></tr>
<tr><td>$v > 200\ km/h$</td><td rowspan="4">$2 \cdot t_2$</td><td rowspan="4">$2 \cdot t_3 + t_4 + t_5$</td><td>10</td><td>90</td><td>10</td></tr>
<tr><td>$v \leq 200\ km/h$</td><td>5</td><td>100</td><td>10</td></tr>
<tr><td>Freight traffic</td><td>5</td><td>220</td><td>10</td></tr>
<tr><td>Urban traffic</td><td>2.5</td><td>50</td><td>5</td></tr>
</table>

Figure 2: The test cycle of the rotational speed for bearings

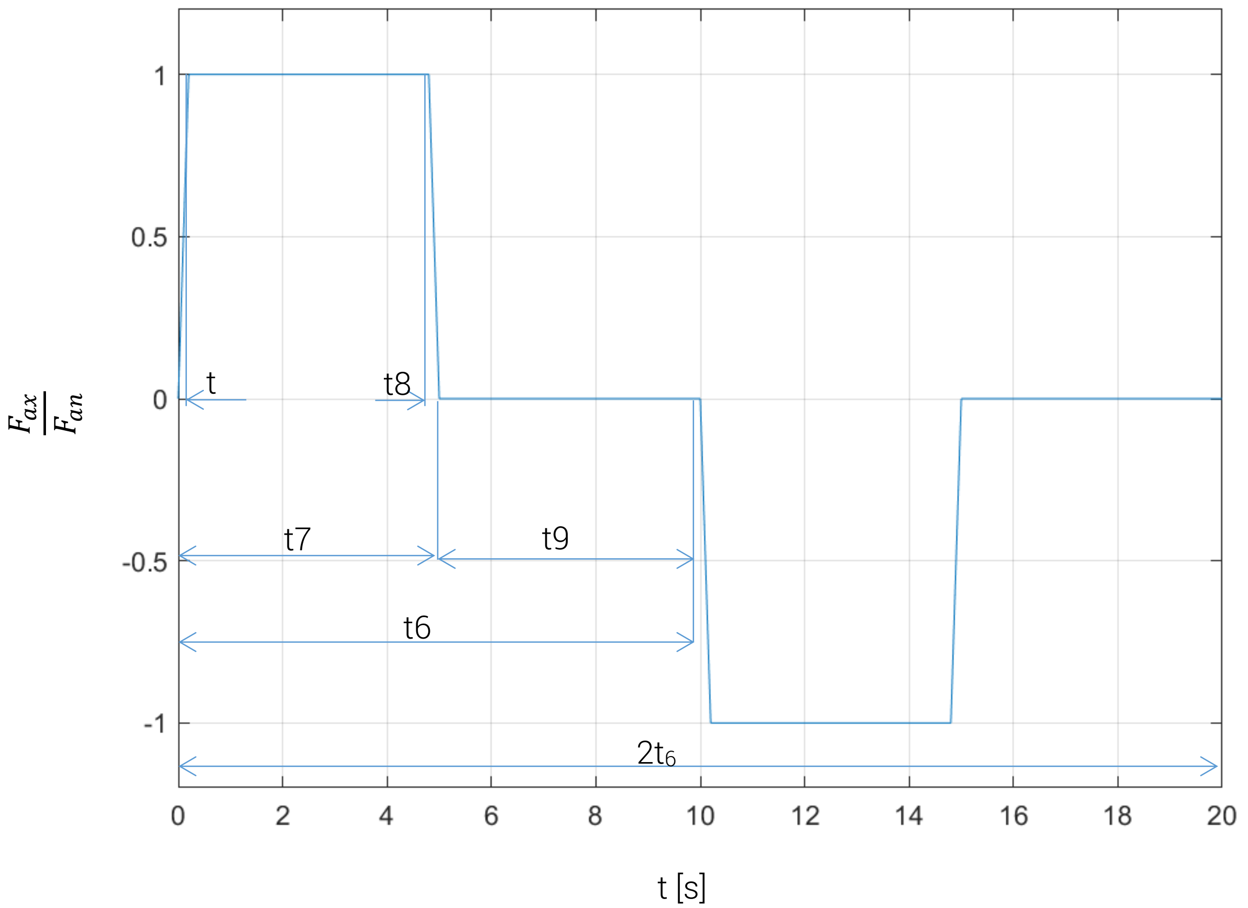

<table>
<tr><td rowspan="2">v_{max}</td><td colspan="4">Time</td></tr>
<tr><td>t6 [s]</td><td>t7 [s]</td><td>t8 [s]</td><td>t9 [s]</td></tr>
<tr><td>$v > 200\ km/h$</td><td rowspan="4">$t_7 + t_9$</td><td rowspan="4">5</td><td rowspan="4">0.2</td><td>0-10</td></tr>
<tr><td>$v \leq 200\ km/h$</td><td>0-10</td></tr>
<tr><td>Freight traffic</td><td>0-5</td></tr>
<tr><td>Urban traffic</td><td>0-5</td></tr>
</table>

Figure 3: The text cycle of axial force for bearings

3.1.2. The investigated characteristics of the bearing

The performance of the investigated bearing during the tests is characterised based on three investigations. These include the following.

1. The temperature of the bearing is monitored during the whole test. Thereby it is investigated in detail that certain limits of the temperature difference are not exceeded. For the investigation performed here the values are not important and can be found in the standard.
    a. The absolute temperature of the bearing
    b. The difference of temperature in one bearing
    c. The difference in temperature between the two bearings
2. The bearing has to be disassembled after the tests and has to be investigated regarding damage incurred. A list of described tolerable damage is given in the standard.
3. The grease has to be investigated regarding its chemical composition. Certain limits of components such as the iron content are specified in the standard.

3.2. EN 13913: elastomer-based mechanical parts in rubber suspension components

Standard EN 13913 is applicable to elastomer-based components designed to be fitted on railway vehicles running on dedicated tracks with permanent guide systems, whatever the type of rail and the running surface.

Typical applications of elastomer-based components include:

a) vehicle suspension systems;
b) equipment mounting systems;
c) joints (e.g.: end-mountings of dampers, elastomer-based bearings and elastomer-based parts used on mechanical joins);
d) limit stops.

These components can be:

I. made entirely of elastomer, operating on their own or in combination with other elastic parts;
II. made up of elastomer and other materials, adherent together or not.

The standard describes the characteristics to be tested as well as proposals for the corresponding test cycles. Characteristics and tests considering influences other than mechanical loads are not described in this chapter since those influences cannot be investigated by performing multibody simulations.

3.2.1. The investigated characteristics of the elastomeric components

Any characteristics of elastomeric components should be defined according to instructions of the present European Standard, i.e. every elastomeric component should comply with the specified criteria. Due to the different possible degradations, an elastomeric component can experience, multiple mechanical characteristics must be tested according the investigated standard. Recommended tolerances are given in Annex C of EN 13913. The standard itself distinguishes between general characteristics and functional characteristics. Elastomeric components characteristics should be selected among these specified in Table A and Table B from this standard.

Table 2: Characteristics of elastomeric components

Characteristic	Characteristic definition (sub-clause)	Inspection and test method (sub-clause)
Resistance to environmental conditions		
Low temperature	6.2.2	7.2.2
High temperature	6.2.3	7.2.3
Ozone	6.2.4	7.2.4
Oil and petroleum products	6.2.5	7.2.5
Chemical product	6.2.6	7.2.6
Abrasion	6.2.7	7.2.7
Fire behaviour	6.2.3	7.2.3
Corrosion	3.2.9	7.2.9
Other conditions	6.2.10	7.2.10
Resistance to operating conditions		
Fatigue resistance	6.3.1	7.3.1
Static creep	6.3.2	7.3.2
Dynamic creep	6.3.3	7.3.3
Static relaxation	6.3.4	7.3.4
Dynamic relaxation	6.3.5	7.3.5
Other conditions	6.3.6	7.3.6
Physical characteristics		
Materials	6.4.1	7.4.1
Mass	6.4.2	7.4.2
Geometrical and dimensional characteristics		
Space envelope	6.5.1	7.5.1
Dimensions	6.5.2	7.5.2

Table 3: Functional characteristics of elastomeric components

Functional characteristic	Characteristic definition (sub-clause)	Inspection and test method (sub-clause)
Characteristics "force as a function of displacement" at constant velocity		
In a new condition	6.6.3.2	7.6.3.2
After test	6.6.3.3	7.6.3.3
Stiffnesses under sinusoidal motion		
In new condition	6.6.4.2	7.64.2
After test	6.6.4.3	7.64.3
Other characteristics		
Dimensions under load	6.6.1	7.6.1
Force under deformation	6.6.2	7.6.2

While the general characteristics include the characteristic behaviour of the component regarding certain external conditions, this characteristic behaviour is to be described by the functional characteristics. Therefore, the general characteristics are investigated by the test cycles described later on while the functional characteristics describe the state of the component itself. The functional characteristics regarding the standard are as follows.

1. The force as a function of the deformation with a constant velocity is measured at the third increase of the deformation with constant velocity. The resulting forces during the increase of the deformation need to be considered rather than the ones during the decrease of the deformation. The limits of this characteristic can be given as maximal and minimal relation between force and deformation.
2. The stiffness under sinusoidal excitation can be considered in three ways: as depending on the amplitude of the displacement, as depending on the amplitude of the force and as depending on the frequency of the excitation. For each of the cases, a predefined amplitude of displacement or force is applied in a sinusoidal form. For the dependency on the frequency, the frequency is varied while it is constant for the other two investigations. The stiffness is measured as the ratio between force and deformation of the component.
3. The damping, similarly to the stiffness under sinusoidal excitation, can be investigated in the three ways already explained. During these experiments, the phase angle between deformation and transmitted force is determined as the damping of the component.
4. The geometry under applied load has to be measured in the fourth cycle of applying a force with a constant velocity at a certain level F_L, which must be specified. Thereby the following relation must apply $F_L < F_M$.

5. The force under deformation is determined similarly to the geometry under applied load. While the component is deformed to a certain maximal deformation L_M with a constant velocity, at a certain deformation L_D the force is measured. The measurement takes place in the fourth cycle of deformation and can be done during the increase or the decrease of the deformation.

3.2.2 The proposed test cycles

The components should be able to withstand stresses and forces to which they are subjected when operating. The fatigue resistance of a component can be evaluated by a fatigue test simulating the displacements and forces encountered in service. EN 13913 describes the two fatigue test methods, which can be used as a basis to draw up the fatigue test of the elastomer components defined in the technical specification.

3.2.2.1. "Staircase" method

The test consists in applying loading sequences to the component, which are the addition of a quasi-static force F_q and a dynamic force F_d varying in time (see Figure 4).

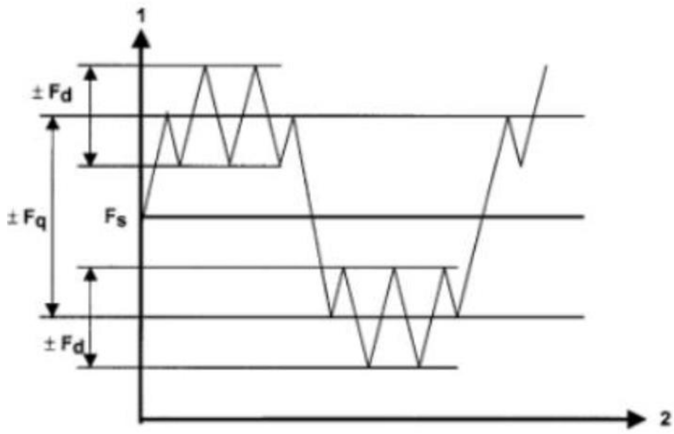

Figure 4: Schematic representation of the load applied in the "staircase" method

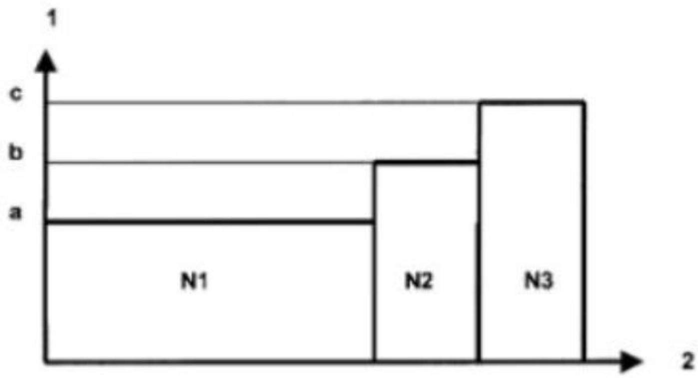

Figure 5: The number of cycles applied within the "staircase" method

The values of force F_q and force F_d as well as the frequency are to be defined in the technical specification.

In the absence of any indication, the following values are used:

$$a = (F_q + F_d);$$
$$b = 1.2 \cdot (F_q + F_d);$$
$$c = 1.4 \cdot (F_q + F_d);$$
$$N1 = 6 \cdot 10^6;$$
$$N2 = 2 \cdot 10^6;$$
$$N3 = 2 \cdot 10^6.$$

Similar to this test the displacement of the component can be applied with the same procedure.

3.2.2.2. "Programming blocks" method

This fatigue test consists of the following stages.

1. Line test
   Measurement of the loads to which the elastomer component is submitted when operating.
2. Load distribution
   Generation of the load distribution, using the "peak counting" method i.e. a peak is counted between two zero crossings (in general, the mean is zero).
3. Blocks
   Classifications on the loads into 8 blocks (recommended number).
4. Sequence
   Determination of the fatigue test programme in sequence, as is shown in Figure 6.

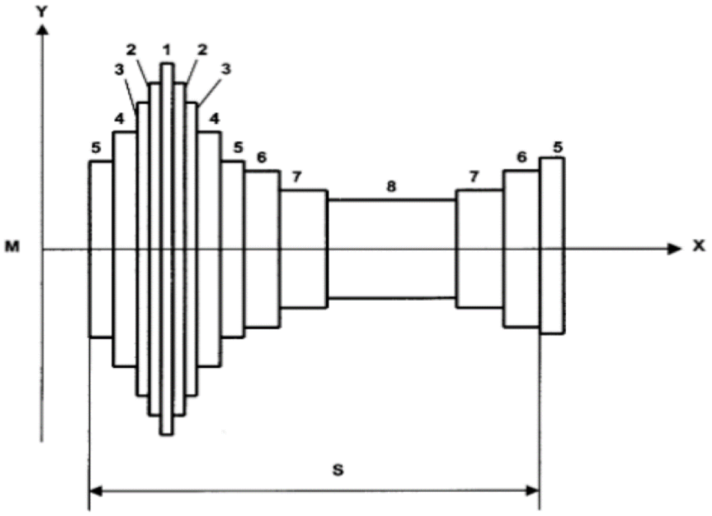

Figure 6: The "Programming blocks" methods

Each sequence is reproduced on a component submitted for testing. The number of sequences should be determined beforehand so as obtain the expected number of kilometres. The test should be continued until destruction of component to estimate its life-time expectancy.

The test cycles given in the standard are proposed for the investigation. Therefore, another design of the test cycles could be used. For this deliverable, the given proposals are investigated.

3.2.3 The proposed limits of the component characteristics

Tolerances and acceptance criteria must be identified in the technical specification of the component. Practical limits should not exceed the limits shown in EN 13913 (Tables C.1, C.2, C.3 and C.4)

Table 4: Permissible variation of characteristics "force as function of displacement" after testing in relation to measurements under new condition.

	Close Criteria	Normal Criteria
Static creep	$\pm 10\%$	$\pm 20\%$
Dynamic creep	$\pm 15\%$	$\pm 20\%$
Static relaxation	$\pm 10\%$	$\pm 20\%$
Dynamic relaxation	$\pm 15\%$	$\pm 20\%$
Heat ageing	$\pm 15\%$	$\pm 20\%$

Table 5 Permissible variation of characteristics "stiffness under sinusoidal motion" after testing in relation to measurements under new condition.

	Close Criteria	Normal Criteria
Static creep	$\pm 15\%$	$\pm 20\%$
Dynamic creep	$\pm 15\%$	$\pm 20\%$
Static relaxation	$\pm 15\%$	$\pm 20\%$
Dynamic relaxation	$\pm 15\%$	$\pm 20\%$
Heat ageing	$\pm 20\%$	$\pm 25\%$

4.The used operation scenario

4.1. Track design

From the track to be simulated described in IMPACT-1 the following representative scenarios may be derived. The track curvature and the running velocity are given by the project IMPACT-1. The data are shown in Figure 7. A curve radius of 0 m marks a straight track.

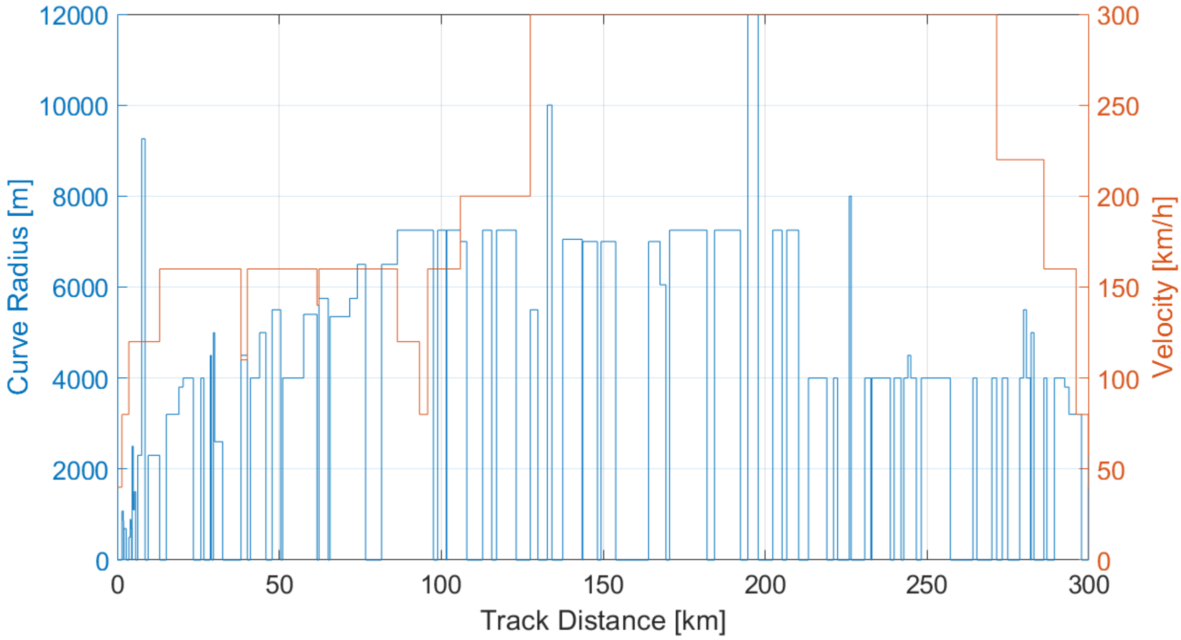

Figure 7: The track given by IMPACT-1.

From this data, the distribution of the fraction of occurring curve radii over the track length is shown in Figure 8 with a class width of 1000m. The class of 13000 *m* contains every part of the track given as straight. For the following simulation scenarios, the smallest radii of the class of *500* m to 1500 *m* are considered as one class although the fraction of track with these radii is quite small. Still, it can be expected that the occurring loads are the highest and therefore it needs to be investigated in detail. It represents the area around stops where the vehicle runs at relatively low speed. The next classes are from 1500 *m* up to 4500 *m* and from 4500 *m* to a straight track. For those three classes representative scenarios are developed.

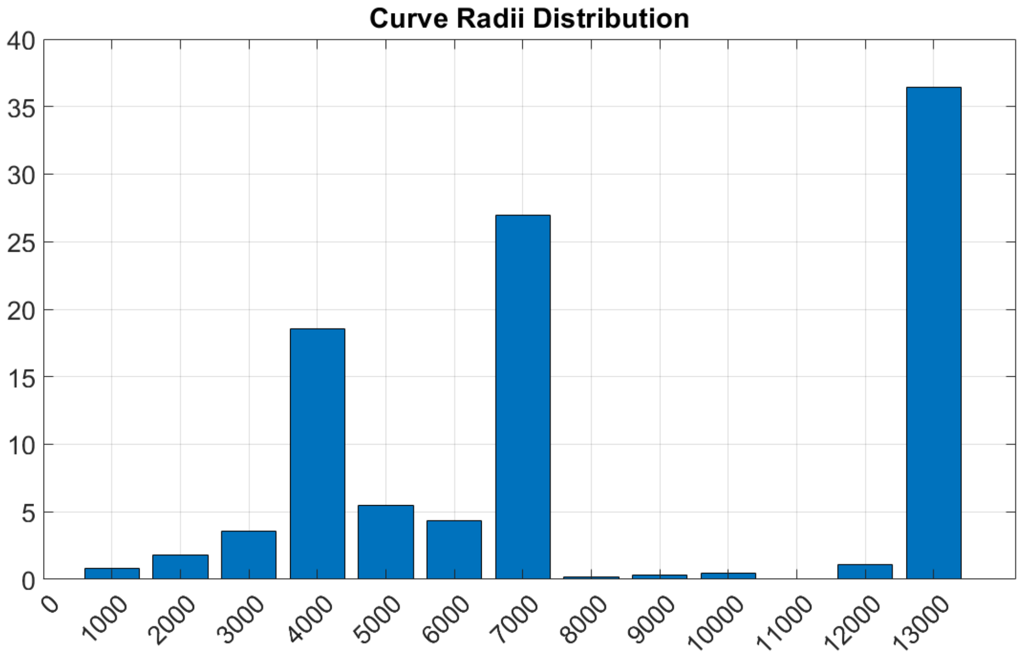

Figure 8: The resulting curve radius distribution.

For each of the described classes the running speeds as well as the superelevation need to be determined. For the low-radius class 1, the speed is varied from 0 to 80 km/h to include accelerating and braking. For class 2 describing intermediate radius curves, a speed of 200 km/h is kept constant and for the high-speed class the speed is set to 300 km/h.

Table 6: The investigated track classes.

Class	Radius	Fraction	Velocity
1	$R < 1500\ m$	0.81 %	0-80 km/h
2	$1500\ m \leq R < 4500\ m$	23.87 %	200 km/h
3	$4500\ m \leq R$	75.32 %	300 km/h

From these conditions the following three simulation scenarios are derived. Superelevation is applied to keep the lateral acceleration according to the standards.

4.1.1. Scenario Class 1

This scenario is added to consider curve radii occurring in the depot and in the proximity of stations (300 m and 800 m). The variations of curvature and superelevation, although not representative of actual tracks in service, allows different conditions to be explored within one simulation including traction and braking.

<table>
<tr><td>Track curvature [1/m]</td><td>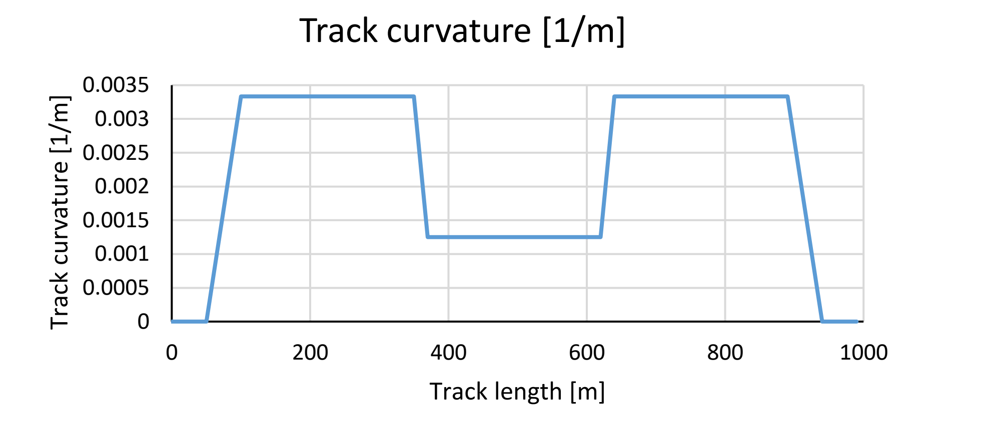
</td></tr>
<tr><td>Superelevation [mm]</td><td>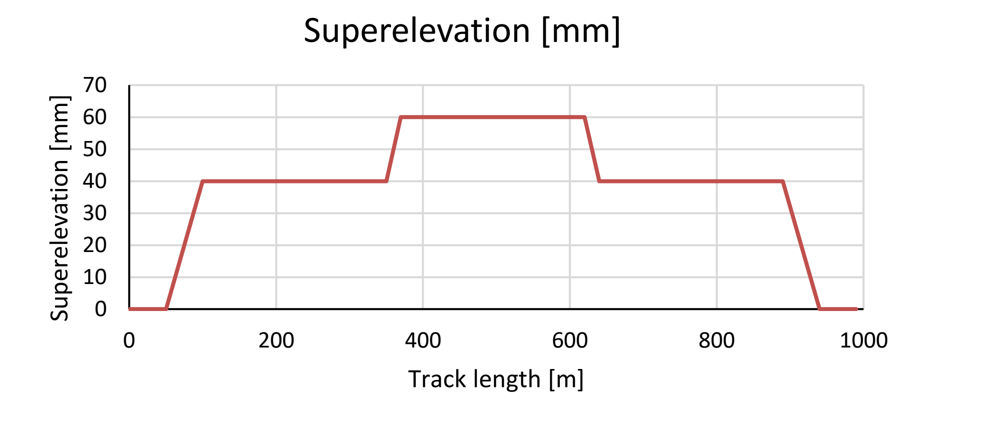
</td></tr>
<tr><td>Velocity [km/h]</td><td>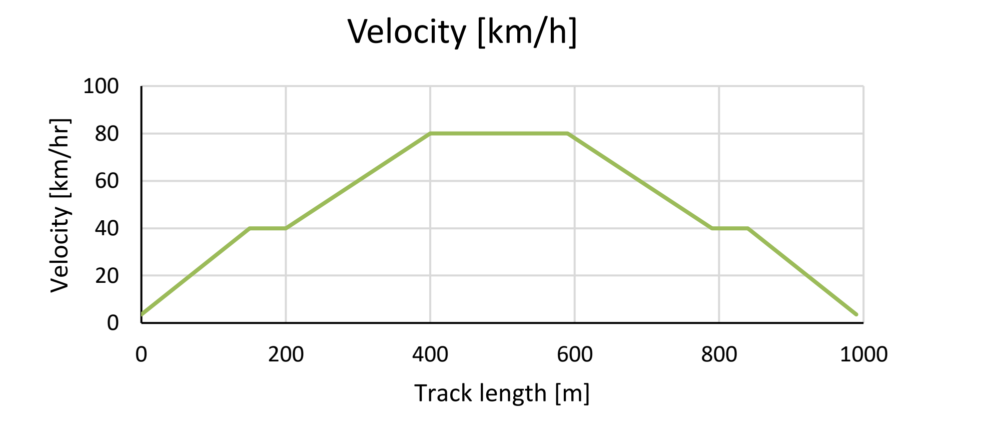
</td></tr>
</table>

Figure 9: Track composition of scenario 1.

4.1.2. Scenario Class 2

<table>
<tr><td>Track curvature [1/m]</td><td>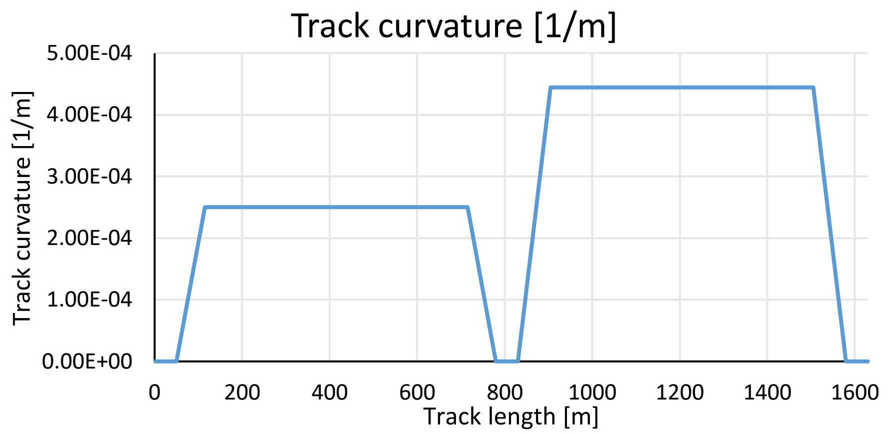
</td></tr>
<tr><td>Superelevation [mm]</td><td>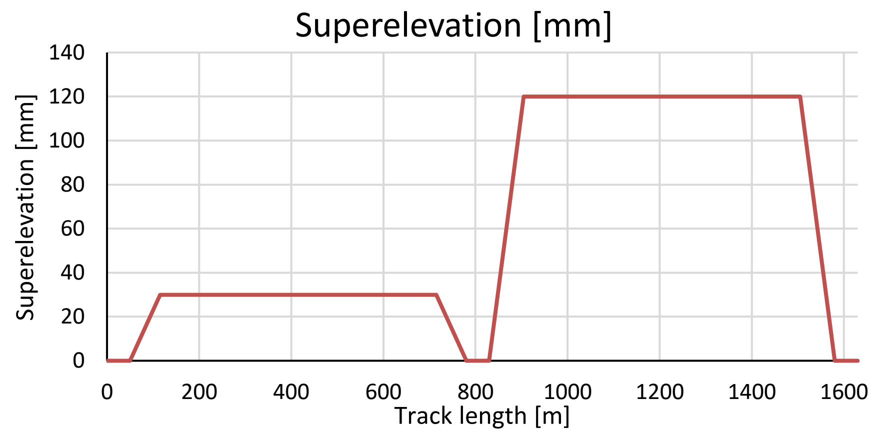
</td></tr>
<tr><td>Velocity [km/h]</td><td>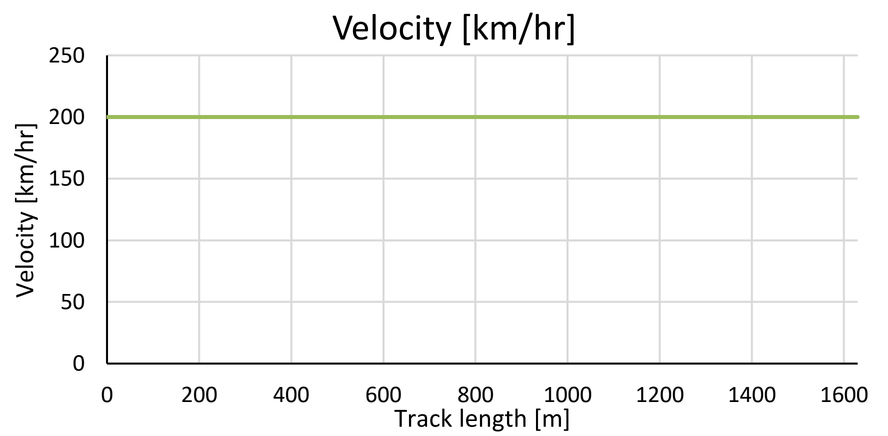
</td></tr>
</table>

Figure 10: Track composition of scenario 2.

4.1.3. Scenario Class 3

Track curvature [1/m]	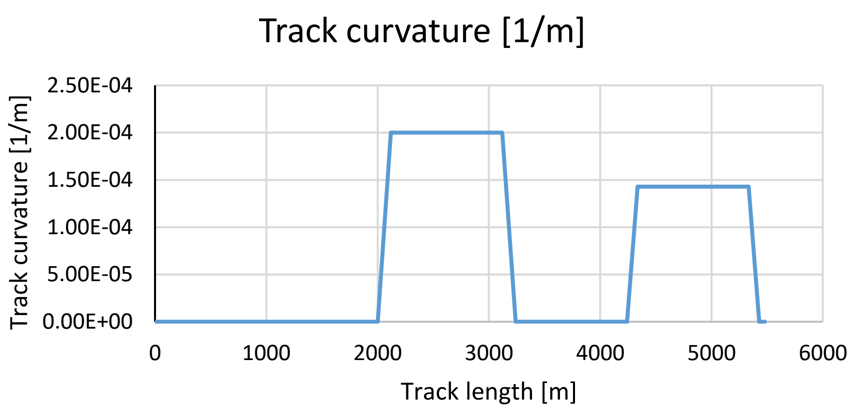
Superelevation [mm]	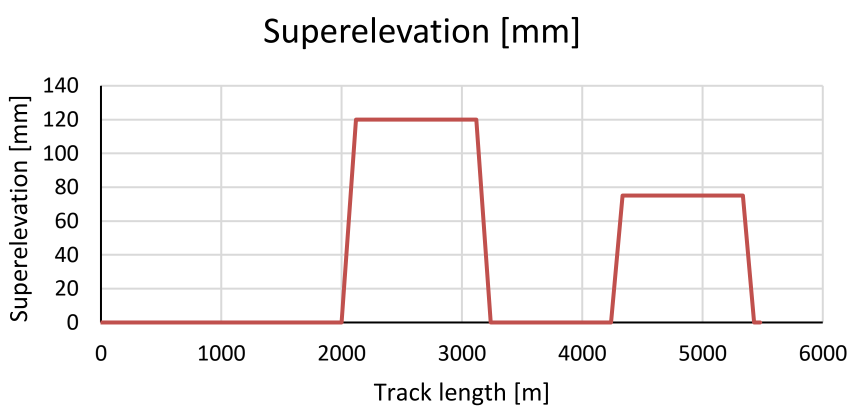
Velocity [km/h]	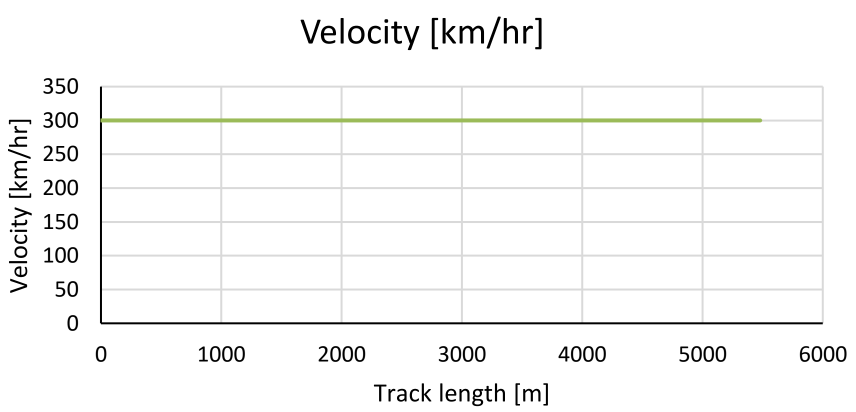

Figure 11: Track composition of scenario 3.

5. Modelling of the vehicle

5.1. The used vehicle parameters

To simulate a highspeed vehicle a suitable set of parameters is chosen. For investigations of the development of polygonised wheels, the German Research Society (Deutsche Forschungsgemeinschaft) published two sets of parameters (Claus et al. 1997). The model to be used refers to the German train ICE 1 with MD 530 bogies. A bogie from the MD 52 family is shown in representative manner in Figure 12 (Baur 2006).

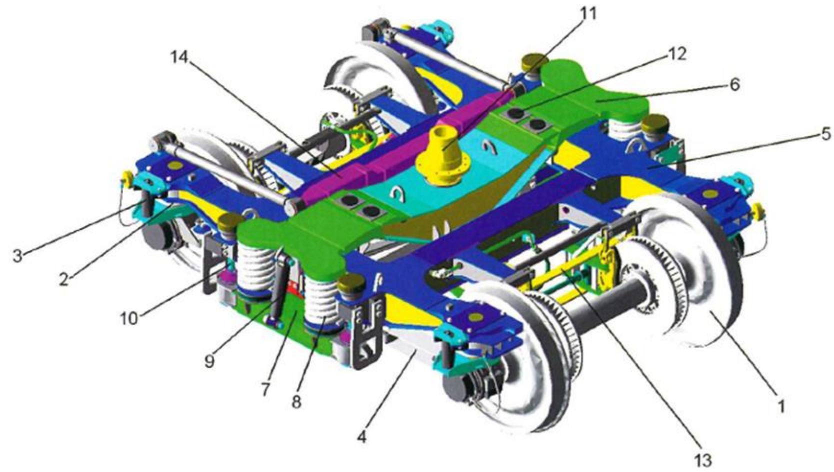

1	Wheel
2	Primary suspension spring
3	Primary damper
4	Axle guidance leaf spring
5	Bogie frame
6	Bolster
7	Spring plank
8	Secondary suspension spring
9	Secondary vertical damper
10	Pendulum link
11	Centre pivot
12	Side bearers
13	Brake rigging
14	Roll bar

Figure 12: The MD 530 bogie (Baur 2006).

From the reference data the parameters of the masses and moment of inertia as well as suspension parameters are implemented in a model in the software Simpack for the investigation of the bearing loads and in Universal Mechanism for the investigation of the elastomeric loads. The primary suspension as well as the secondary suspension and its parameters from the basic model in Simpack are shown in the following figures.

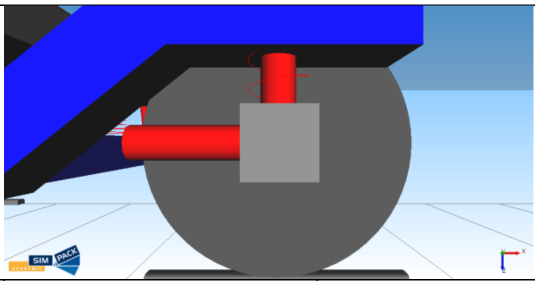			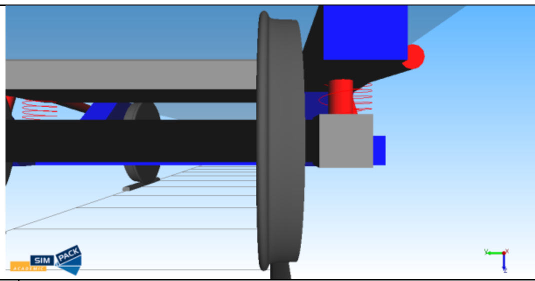	
1	$c_x = 5.2 \cdot 10^7 \frac{N}{m}$	$d_x = 300 \frac{Ns}{m}$	4	$m_{WS} = 1850\ kg$ $I_{xx} = 960\ kgm^2$ $I_{yy} = 85\ kgm^2$ $I_{zz} = 960\ kgm^2$
2	$c_y = 3.5 \cdot 10^6 \frac{N}{m}$	$d_y = 300 \frac{Ns}{m}$		
3	$c_z = 10^6 \frac{N}{m}$	$d_z = 1.2 \cdot 10^4 \frac{Ns}{m}$		
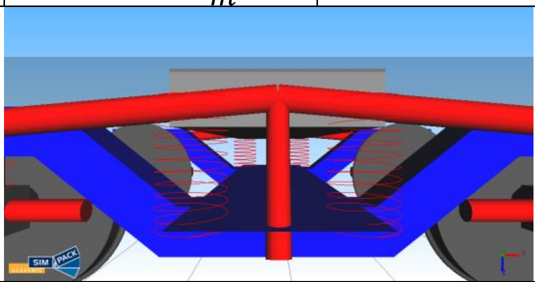			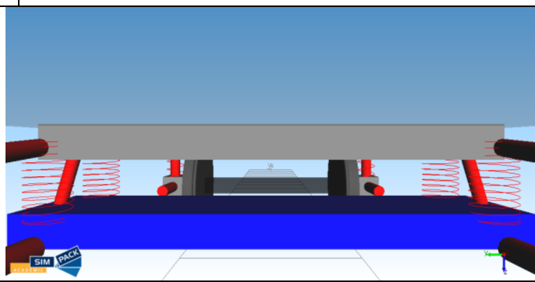	
5	$c_x = 6 \cdot 10^5 \frac{N}{m}$	$d_x = 500 \frac{Ns}{m}$	8	$I_{zz} = 400\ kgm^2$
6	$c_y = 3.5 \cdot 10^5 \frac{N}{m}$	$d_y = 2 \cdot 10^4 \frac{Ns}{m}$	9	$m_{bf} = 2380\ kg$ $I_{xx} = 1924\ kgm^2$ $I_{yy} = 1080\ kgm^2$ $I_{zz} = 2970\ kgm^2$
7	$c_z = 3.5 \cdot 10^5 \frac{N}{m}$	$d_z = 2 \cdot 10^4 \frac{Ns}{m}$		
10	$c_p = 35 \cdot 10^6 \frac{Nm}{rad}$	$d_p = 4 \cdot 10^6 \frac{Nms}{rad}$	11	$m_{vb} = 33106\ kg$ $I_{xx} = 718234\ kgm^2$ $I_{yy} = 1779000\ kgm^2$ $I_{zz} = 1779000\ kgm^2$

Figure 13: The vehicle characteristics given by the data set.

The numbered elements are:

1. Longitudinal primary spring/damper
2. Lateral primary spring/damper
3. Vertical primary spring/damper
4. Wheelset
5. Longitudinal secondary spring/damper
6. Lateral secondary spring/damper
7. Vertical secondary spring/damper
8. Bolster
9. Bogie frame
10. Centre pivot as rotational spring/damper
11. Vehicle body

In detail the according geometry can be found on the website (Claus et al. 1997). Additional it needs to be said that the lateral secondary spring has a clearance of 12.5 *mm* per deviation to one side, resulting from the design as limit stop.

For the two different investigated standards two separate models were built to determine the loads to be tested. To adjust the models to the investigated components both models were separately adapted based on the said publish set of parameters. The adjustment is described separately in the following chapters.

5.2. Model adaptations for simulation of bearing loads

For the model the standard S1002 and UIC 60E2 profiles in new conditions are used for journal bearings investigations. The rail inclination is 1/40 and the Fastsim contact formulation is used to simulate the wheel/rail contact forces.

For the developed simulation scenarios, it is important that the model shows a realistic running behaviour corresponding to the behaviour of a high-speed train at an operating speed of 300 km/h. If the model is not stable at the investigated velocities, unrealistic loads on the bearings, especially in combination with track irregularities, can result. Therefore, its running stability was investigated. After injection of an initial lateral displacement and lateral velocity of the wheelsets, the occurring sinusoidal wheelset motions were investigated. A decreasing amplitude of the motion describes a stable system state while increasing amplitude to the point of flange contact shows an unstable state. For a high-speed vehicle, the critical velocity which defines the change of the system state is above the operating speed by a certain safety margin.

Velocity	Lateral Displacement of the four wheelsets
$v = 80\ \frac{m}{s}$ $(288 \frac{\mathrm{km}}{\mathrm{h}})$	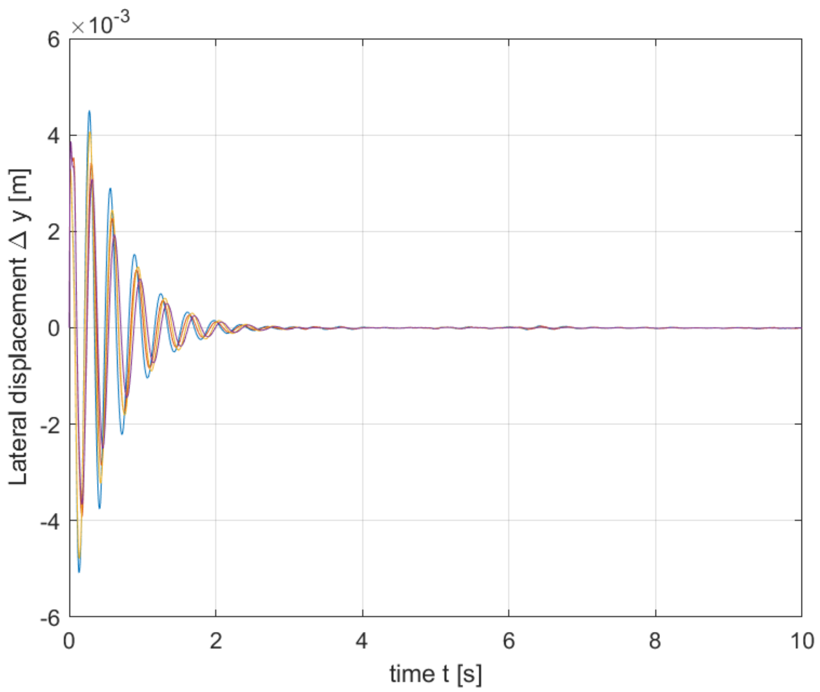

<table>
<tr>
<td>$v = 81\ \frac{m}{s}$
$(291.6\frac{\mathrm{km}}{\mathrm{h}})$</td>
<td>
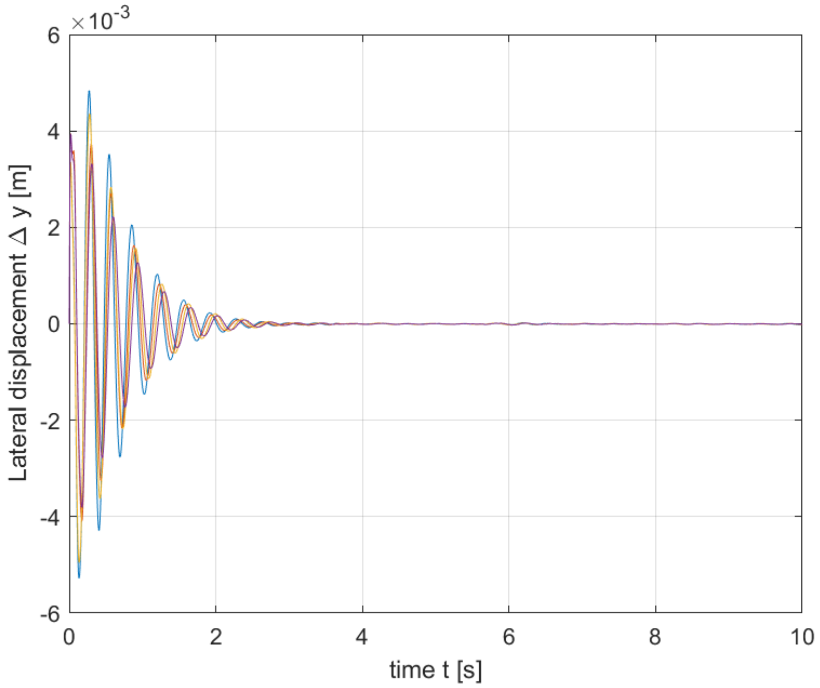

</td>
</tr>
<tr>
<td>$v = 82\ \frac{m}{s}$
$(295.2\frac{\mathrm{km}}{\mathrm{h}})$</td>
<td>
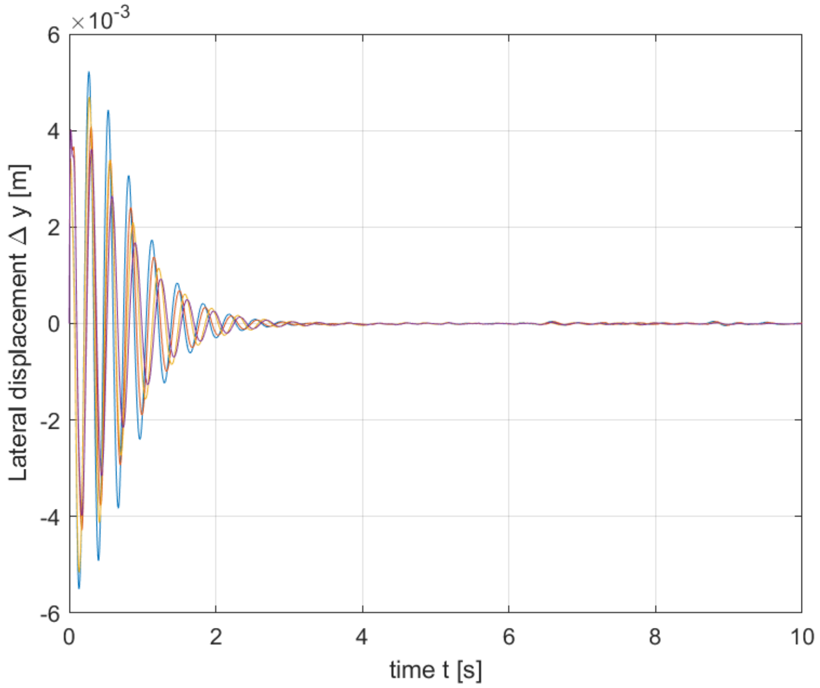

</td>
</tr>
</table>

$v = 83\ \frac{m}{s}$ $(298.8\frac{\text{km}}{\text{h}})$	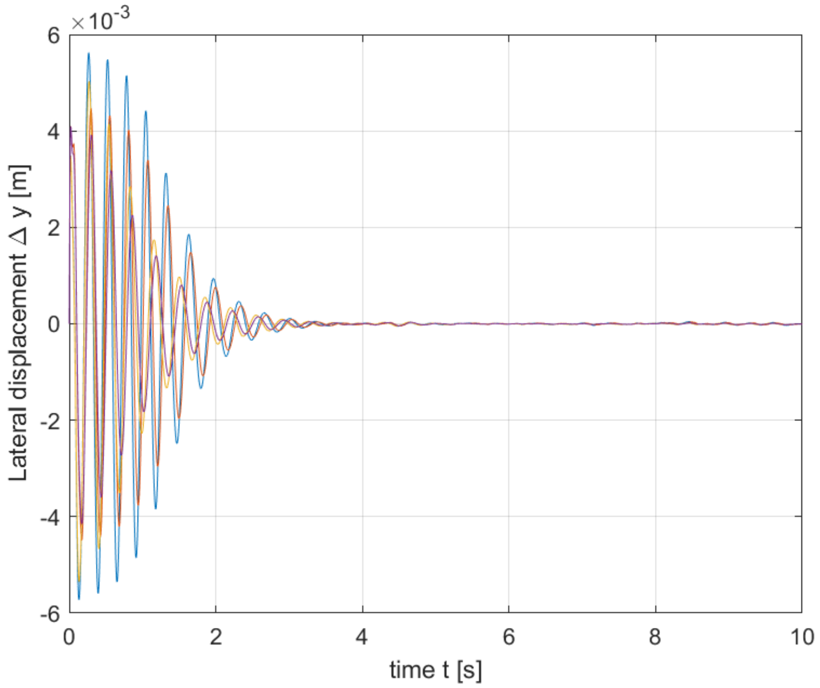
$v = 84\ \frac{m}{s}$ $(302.4\frac{\text{km}}{\text{h}})$	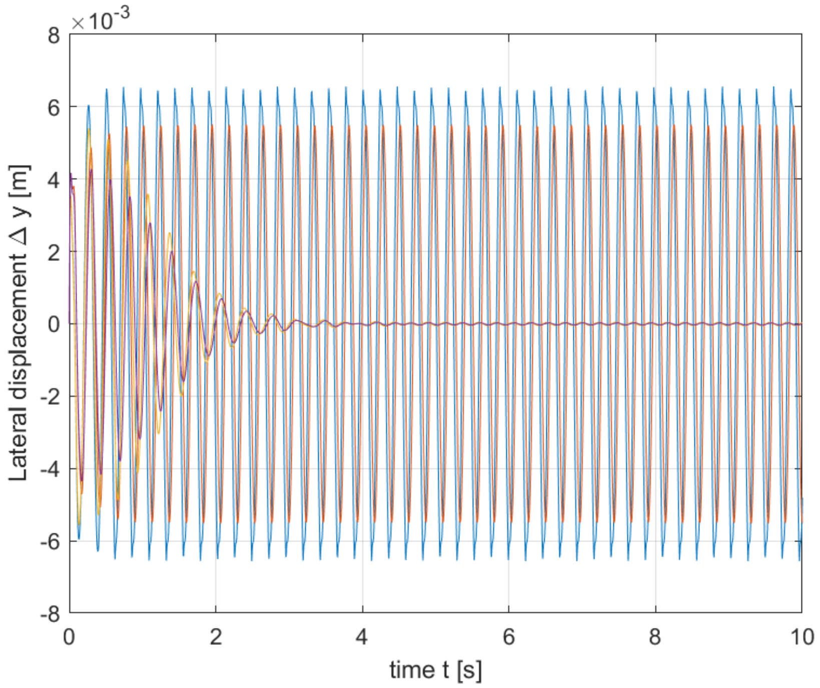

Figure 14: Stability analysis with the base model.

It can be observed that the critical velocity was initially in the range of the aimed speed for simulation scenario 3. Due to the fact that a poor running stability would lead to unrealistically high loads on the bearing, the suspension of the vehicle model was adapted concerning two points to increase the critical velocity.

Firstly, in the given model the secondary lateral springs have a clearance of 25 mm. Before the bogie frame is displaced by this clearance relative to the bolster, no lateral spring is active. Due to the fact that in the real vehicle the secondary vertical springs are coil springs, they can be expected to have a lateral stiffness. The stiffness normal to the main axis of a coil spring can be calculated according to Hanneforth and Fischer (Hanneforth 1986).

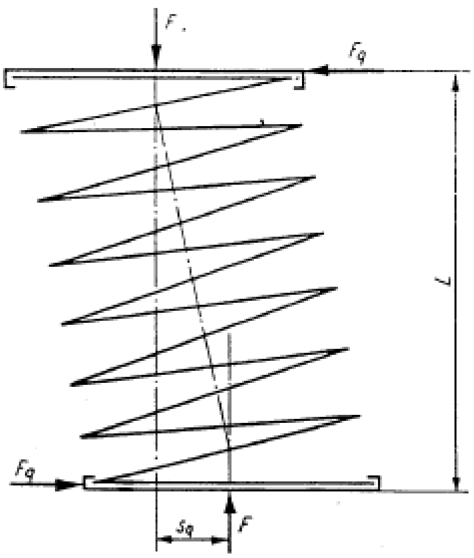

$$c_q = \frac{1}{\frac{1}{F} \cdot \left[\frac{2}{x} \cdot \tan\left(x \cdot \frac{L}{2}\right) - L\right)\Big] + \frac{L}{S}}$$

$$x = \sqrt{\frac{F}{B \cdot \left(1 - \frac{F}{S}\right)}}$$

$$S = 3360 \cdot \frac{L \cdot d^4}{i \cdot r^3}$$

$$B = 1460 \cdot \frac{L \cdot d^4}{i \cdot r}$$

With:

- F the vertical force on the spring
- L the length under the applied force
- i the number of turns
- d the diameter of the wire
- r the radius of the coil

Figure 15: Calculation of the stiffness of a coil spring normal to its axis (Hanneforth 1986).

With a diameter of 35 *mm* of the coil, 6 turns and a radius of *100 mm* the stiffness normal to the axis of the spring results to $c_{x,y} = 25000 \frac{N}{m}$. This normal stiffness is added in the model in longitudinal and lateral direction to gain a lateral stiffness in the secondary suspension before the clearance in the given model is covered.

As a second adaptation, the damping of the rotation around the vertical axis in the secondary suspension was adapted so that the overall damping between bogie frame and vehicle car body corresponds to the damping of the reference data set A rather than the used data set B. Therefore, the configuration of the data set A without bolster is damped against the rotation around the vertical axis as shown in comparison with data set B in the following figure. While dataset A has a secondary suspension with a direct connection between car body and the bogie frame via two longitudinal dampers and two lateral dampers shifted in longitudinal direction dataset B is designed with a bolster and its rotational damping around the centre pivot and longitudinal dampers linking bogie frame and the bolster.

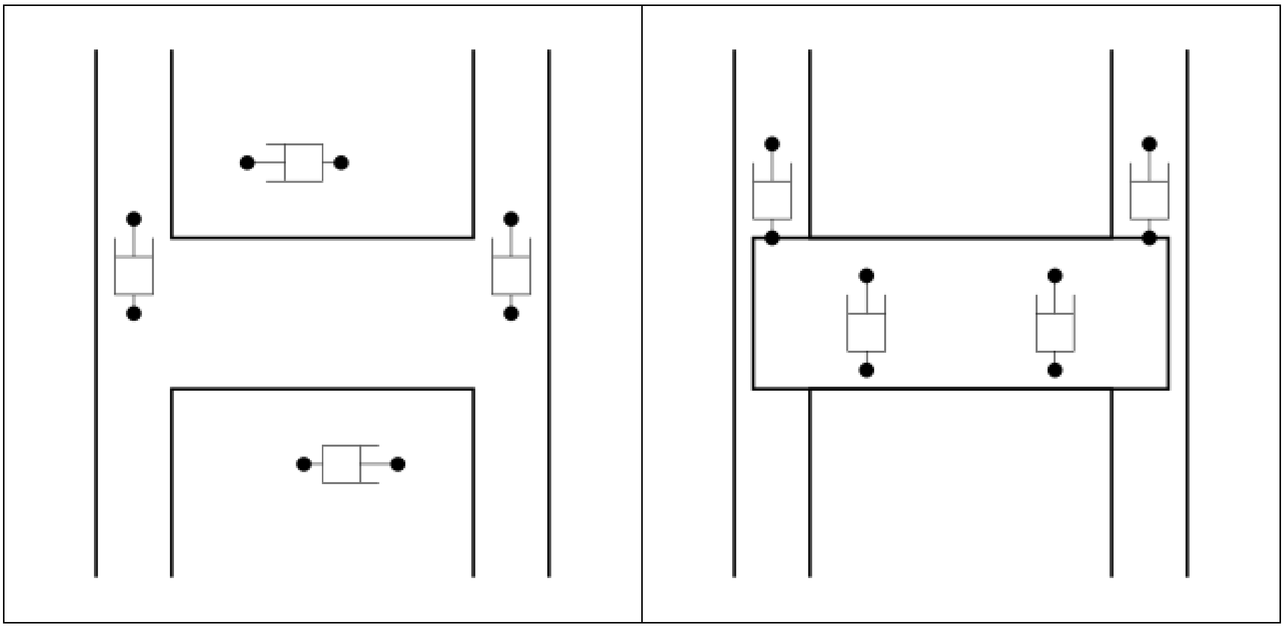

Figure 16: Schematic comparison of the damping configuration on the bogies of reference parameter set A (left) and reference parameter set B (right).

For data set A therefore the damping between bogie frame and car body against the rotational angle φ can be described as:

$$d_{equ,A} \cdot \dot{\varphi} = 2 \cdot a_{d,y}^2 \cdot d_y \cdot \dot{\varphi} + 2 \cdot a_{d,x}^2 \cdot d_x \cdot \dot{\varphi}$$

$$d_{equ,A} = 2 \cdot a_{d,y}^2 \cdot d_y + 2 \cdot a_{d,x}^2 \cdot d_x$$

While for data set B the overall equivalent damping results from the connection between bogie frame and bolster and bolster to car body in serial connection.

$$\frac{1}{d_{equ,B}} = \frac{1}{d_p} + \frac{1}{2 \cdot a_{d,x}^2 \cdot d_x}$$

From the aim to adjust the damping for the vehicle model to the damping behaviour of data set A the damping constant d_x of the secondary longitudinal dampers results as:

$$d_x = \frac{1}{\left(\frac{1}{d_{equ,A}} - \frac{1}{d_p}\right) \cdot 2 \cdot a_{d,x}^2}$$

$$d_x = 254598.6 \frac{Ns}{m}$$

Therefore, the longitudinal damping of the secondary dampers were changed to

$$d_x = 260000 \frac{Ns}{m}$$

The systematic stability was investigated again and the following results could be generated. It is visible that the critical velocity increased and therefore a more realistic investigation of the loads on the bearings can be executed.

Velocity	Lateral displacement of the vehicle
$v = 82\ \frac{m}{s}$ $(295.2 \frac{\text{km}}{\text{h}})$	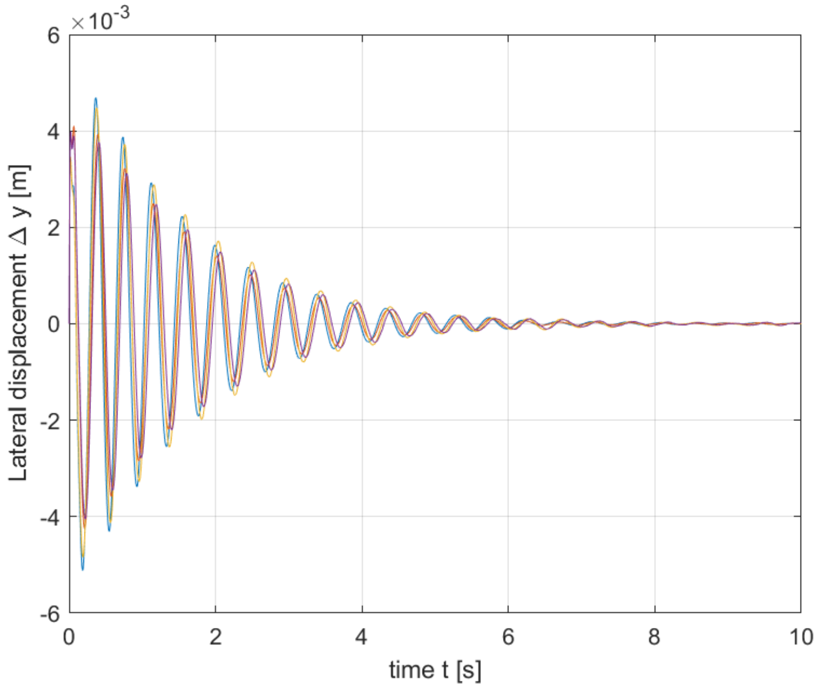
$v = 83\ \frac{m}{s}$ $(298.8 \frac{\text{km}}{\text{h}})$	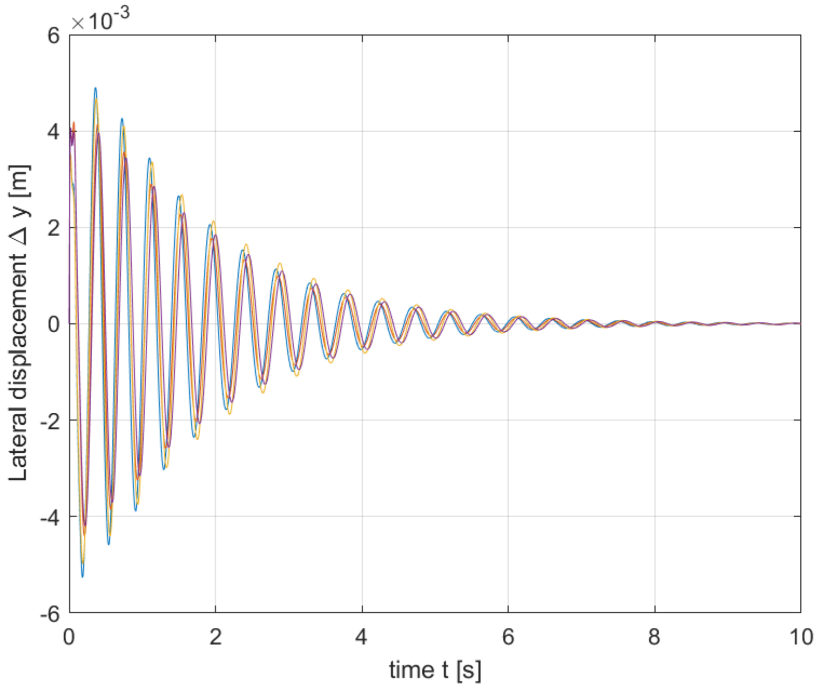

$v = 84\ \frac{m}{s}$ $(302.4\frac{\text{km}}{\text{h}})$	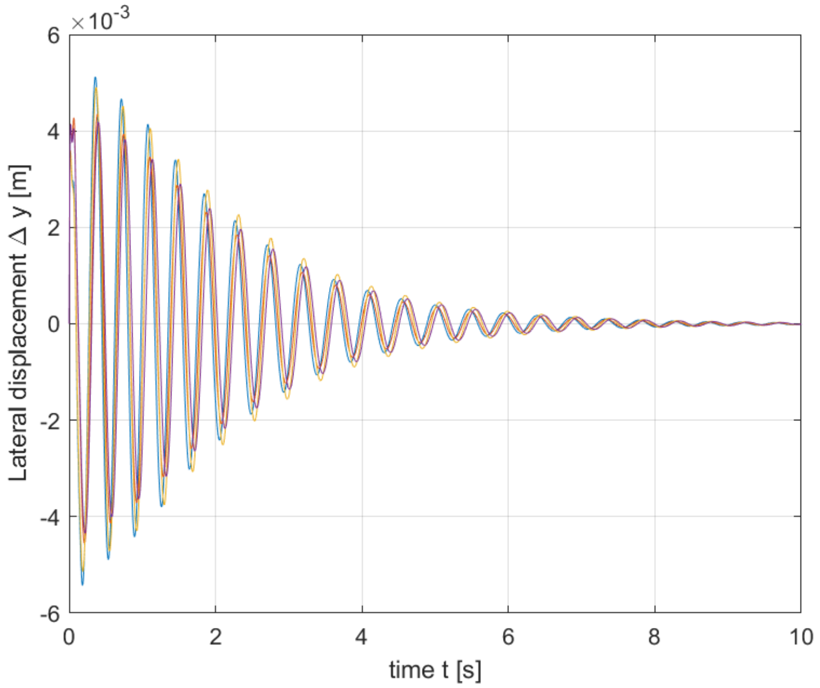
$v = 85\ \frac{m}{s}$ $(306\frac{\text{km}}{\text{h}})$	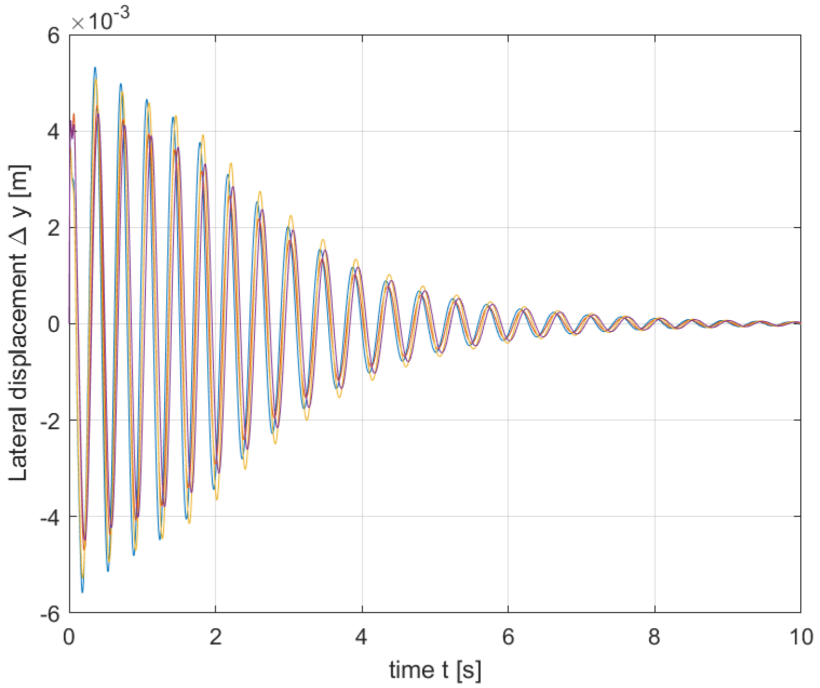

$v = 86\ \frac{m}{s}$ $(309.6\frac{\text{km}}{\text{h}})$	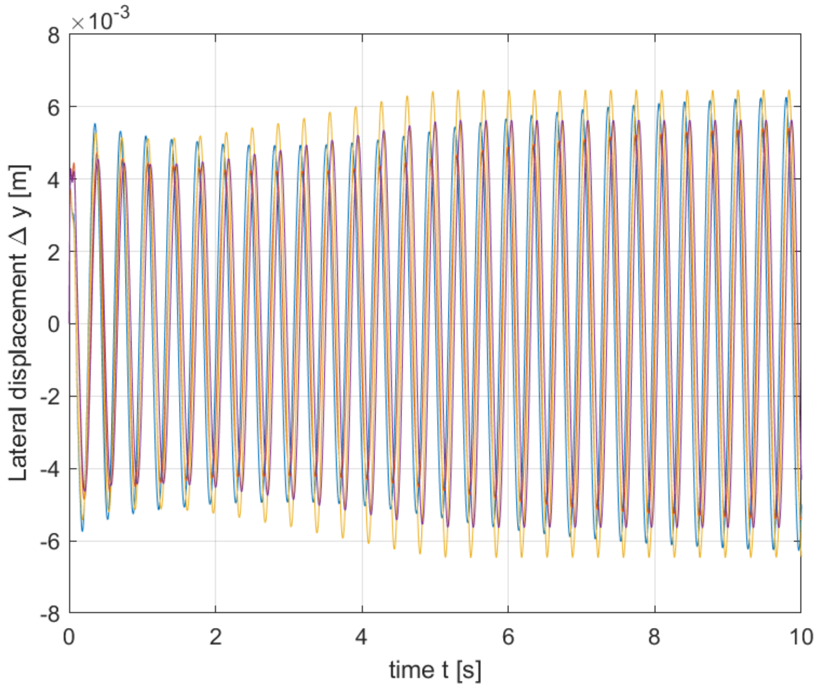

Figure 17: Stability analysis after the first adaption.

5.3. Model adaptation for simulation of elastomer component loads

The bogie is adapted by introducing a swing-arm type primary suspension with an elastomeric bushing connecting the arm to the bogie frame. In this way, a key elastomeric component – the bushing – is introduced.

The swing arm system has several functions including support of the axlebox, connection of the bogie and axlebox, and also transfer of braking and traction force in the longitudinal direction from the axle to the bogie. Elastic bushings are arranged on the link between the bogie and the swing arm to provide controlled lateral movement for the purpose of improving curving performance. The system's vertical, longitudinal, and lateral stiffness can be adjusted according to design requirements and operating conditions to prevent derailment and ensure stable operation at high speed. This configuration is found in metros and intercity trains, but also on high-speed trains like the CRH-1A in China. The approach at this stage of project is replace the coil springs for elastomeric component at primary suspension.

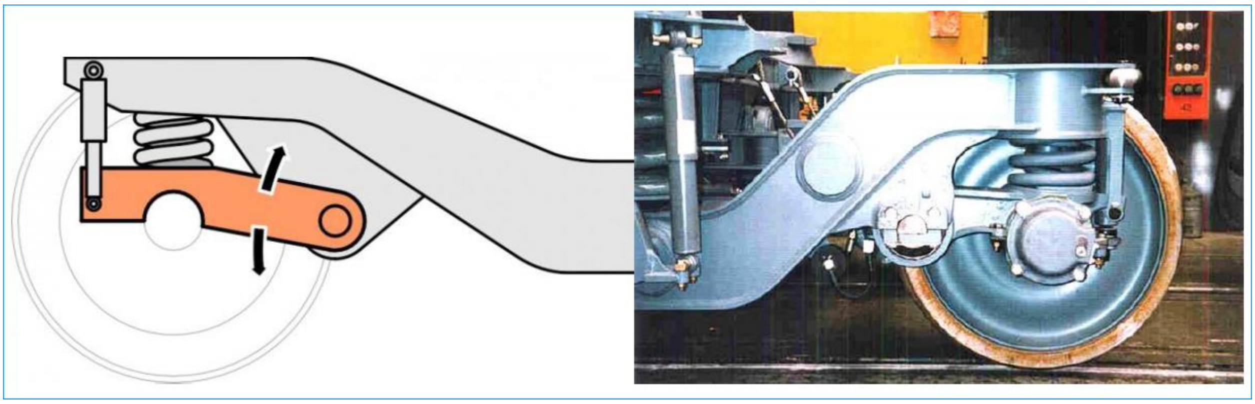

Figure 18: Architecture of the adapted primary suspension, consisting of trailing arm, elastomeric bushing, primary spring, and damper.

From the reference data, the parameters of the masses and moments of inertia, as well as the suspension parameters, are implemented in a model in the Universal Mechanism software for the investigation of bearing loads and elastomeric component loads.

The spring and bushing elements are simulated as linear elements as a preliminary step of the study. The stiffness parameters are presented in form of the following matrix:

$$\begin{bmatrix} K_T & K_{T-R} \\ K_{R-T} & K_R \end{bmatrix}$$

In this matrix, K_T and K_R represent the translational and rotational stiffnesses in the form of a 3 X 3 matrix. There is a coupling effect of the translational movements on the generated rotational moments as represented by the K_{T-R} and K_{R-T} matrixes.

The reaction forces of an elastic component subject to the vector of displacements can be presented as follow:

$$\begin{bmatrix} F_x \\ F_y \\ F_z \\ M_x \\ M_y \\ M_z \end{bmatrix} = \begin{bmatrix} k_{xx} & 0 & 0 & 0 & k_{xx}H/2 & 0 \\ 0 & k_{yy} & 0 & -k_{yy}H/2 & 0 & 0 \\ 0 & 0 & k_{zz} & 0 & 0 & 0 \\ 0 & -k_{xx}H/2 & 0 & k_{\theta} & 0 & 0 \\ k_{yy}H/2 & 0 & 0 & 0 & k_{\beta} & 0 \\ 0 & 0 & 0 & 0 & 0 & k_{\psi} \end{bmatrix} \begin{bmatrix} x \\ y \\ z \\ \theta \\ \beta \\ \psi \end{bmatrix}$$

The primary suspension as well as the secondary suspension and its parameters are shown in Figure 19.

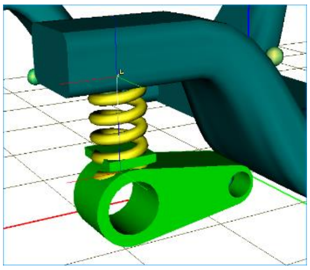			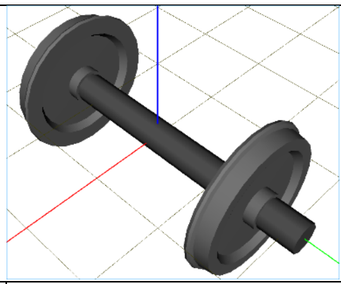	
1	$k_{xx} = 3.5 \times 10^6 \dfrac{N}{m}$	$d_{xx} = 6 \times 10^4 \dfrac{Ns}{m}$	4	$m_{WS} = 1850\ kg$ $I_{xx} = 960\ kgm^2$ $I_{yy} = 85\ kgm^2$ $I_{zz} = 960\ kgm^2$
2	$k_{yy} = 3.5 \times 10^6 \dfrac{N}{m}$	$d_{yy} = 6 \times 10^4 \dfrac{Ns}{m}$		
3	$k_{zz} = 1.0 \times 10^6 \dfrac{N}{m}$	$d_{zz} = 1 \times 10^4 \dfrac{Ns}{m}$		
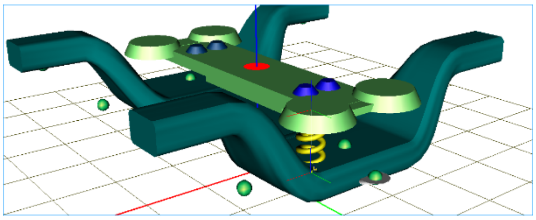			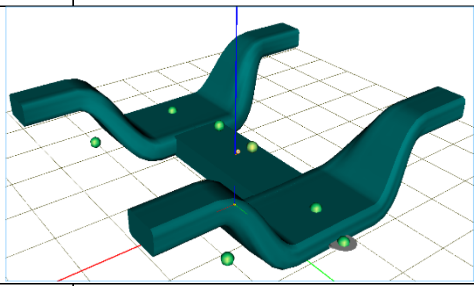	
5	$k_x = 6 \times 10^5 \dfrac{N}{m}$	$d_x = 500 \dfrac{Ns}{m}$	8	$I_{zz} = 400\ kgm^2$
6	$k_y = 3.5 \times 10^5 \dfrac{N}{m}$	$d_y = 2 \times 10^4 \dfrac{Ns}{m}$	9	$m_{bf} = 2380\ kg$ $I_{xx} = 1924\ kgm^2$ $I_{yy} = 1080\ kgm^2$ $I_{zz} = 2970\ kgm^2$
7	$k_z = 3.5 \times 10^5 \dfrac{N}{m}$	$d_z = 2 \times 10^4 \dfrac{Ns}{m}$		
10	$k_p = 35 \times 10^6 \dfrac{Nm}{rad}$	$d_p = 4 \times 10^6 \dfrac{Nms}{rad}$	11	$m_{vb} = 33106\ kg$ $I_{xx} = 718234\ kgm^2$ $I_{yy} = 1779000\ kgm^2$ $I_{zz} = 1779000\ kgm^2$

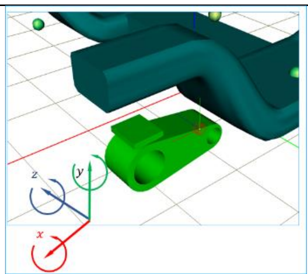		
12	$k_x^{tArm} = 5 \times 10^6 \dfrac{N}{m}$	$c_x^{tArm} = 1 \times 10^6 \dfrac{Ns}{m}$
13	$k_y^{tArm} = 5 \times 10^6 \dfrac{N}{m}$	$c_y^{tArm} = 1 \times 10^6 \dfrac{Ns}{m}$
14	$k_z^{tArm} = 5 \times 10^6 \dfrac{N}{m}$	$c_z^{tArm} = 1 \times 10^6 \dfrac{Ns}{m}$
15	$k_{rot.x}^{tArm} = 1 \times 10^5 \dfrac{Nm}{rad}$	$c_{rot.x}^{tArm} = 1 \times 10^5 \dfrac{Nms}{rad}$

16	$k_{rot.y}^{tArm} = 0\ \frac{Nm}{rad}$	$c_{rot.y}^{tArm} = 10\ \frac{Nms}{rad}$
17	$k_{rot.z}^{tArm} = 1 \times 10^5\ \frac{Nm}{rad}$	$c_{rot.z}^{tArm} = 1 \times 10^5\ \frac{Nms}{rad}$

Figure 19: Model parameters adapted for the simulation of elastomer component loads.

The numbered elements are:

1. Longitudinal primary spring/damper
2. Lateral primary spring/damper
3. Vertical primary spring/damper
4. Wheelset
5. Longitudinal secondary spring/damper
6. Lateral secondary spring/damper
7. Vertical secondary spring/damper
8. Bolster
9. Bogie frame
10. Centre pivot as rotational spring/damper
11. Vehicle body
12. Longitudinal stiffness and damping of trailing arm bushing
13. Lateral stiffness and damping of trailing arm bushing
14. Vertical stiffness and damping of trailing arm
15. Rotational stiffness and damping of trailing arm about longitudinal axis
16. Rotational stiffness and damping of trailing arm about lateral axis
17. Rotational stiffness and damping of trailing arm about vertical axis

The vertical damper, shown as item 3 in Figure 20 is simulated as a bi-linear vertical damper as follows.

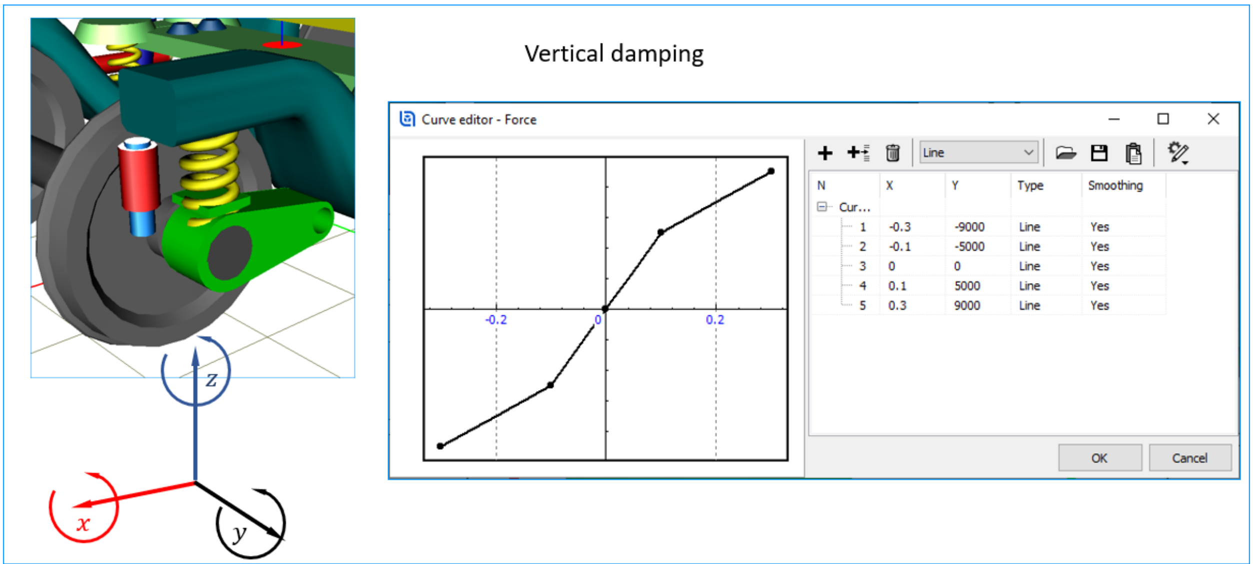

Figure 20: Bi linear damper in the primary suspension of the bogie.

5.3.1. A virtual characterization rig of suspension element

As an alternative approach to a full three-dimensional model of the full coach, a virtual test rig is developed in Universal Mechanism software. The virtual rig has the ability of isolating the forces of the wheel/rail contacts and the movements of the track and generally isolate the system. At this stage, this model is not going to replace the full 3D MBS model but is a tool to evaluate the force response of the elastomeric elements as individual or integrated systems but without the wheel/rail effects.

The Figure 21 shows a developed virtual test rig at this stage. The shown axle box is subject to sinusoidal lateral movements and the different forces and displacements generated in the elastomeric components are presented.

The elastomeric spring is graphically represented by a helical coil, but mechanical characteristics are close to an initial values of stiffness and damping presented in 5.1

Despite the linear stiffnesses characterising the elements, different nonlinear stiffening behaviours are observed for the F_x and M_x directions.

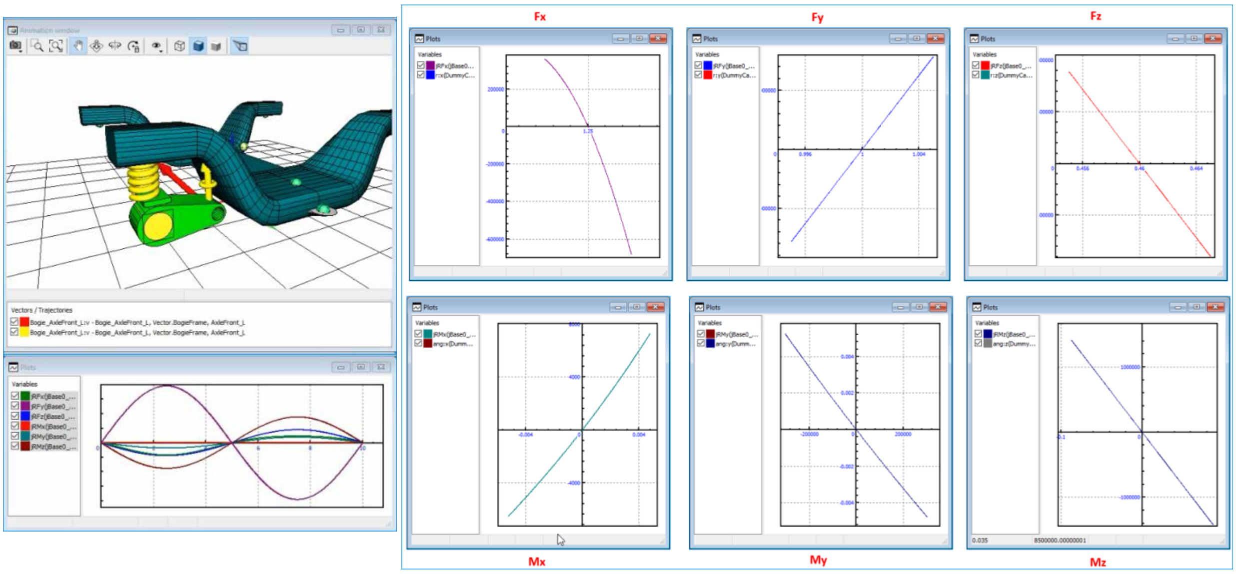

Figure 21: The virtual rig and the response of the system subjected to harmonic displacements of the trailing arm.

At this stage of the project, the usage of the test rig is limited to double checking the response of the elastomeric component, but it could be extended further.

5.3.2. Full MBS model

The MBS system of the bogie developed in Universal Mechanism is shown in Figure 22

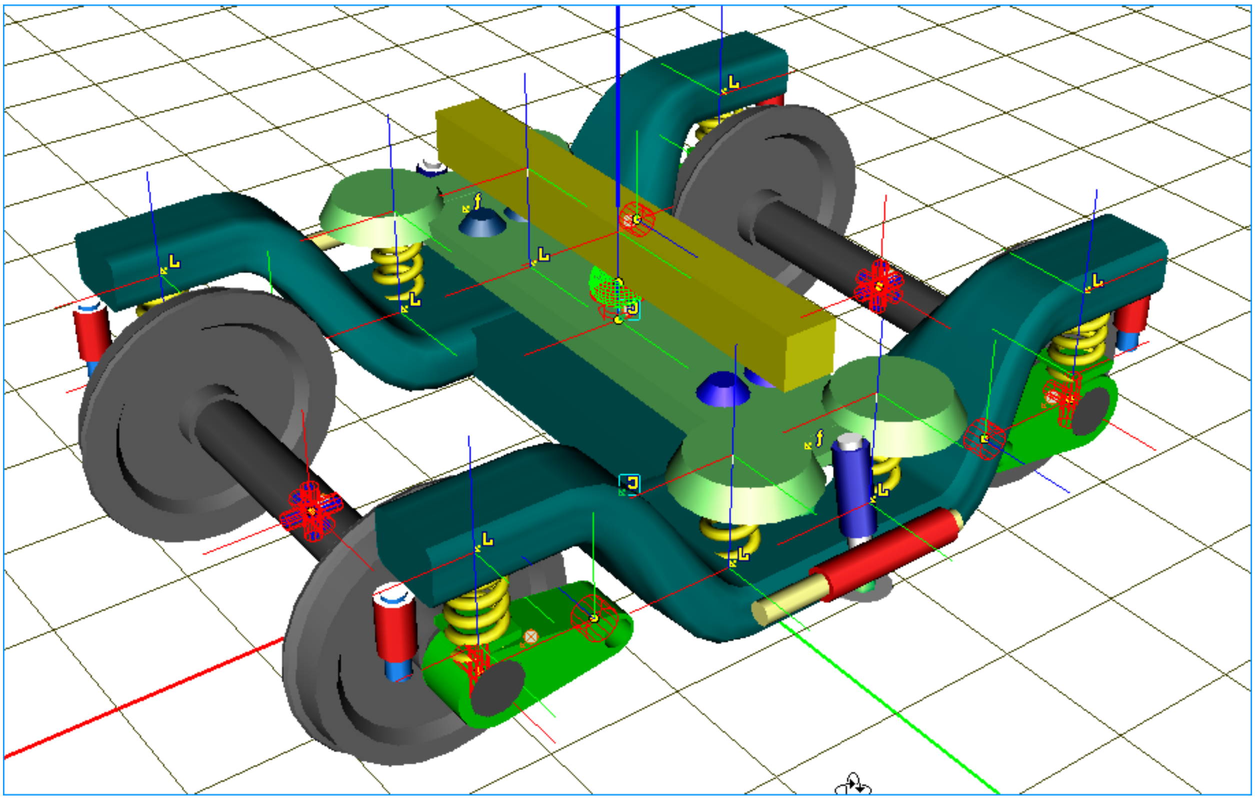

Figure 22: Schematic view of the bogie as developed with the Universal Mechanism software.

The total degrees of freedom (DoF) of the system, comprising two bogies and one car body, is 70 DoF.

5.3.3. Wheel and rail contact

The standard S1002 and UIC 60 profiles in new conditions are used for the simulation of full MBS model. The rail inclination is set to 1/40 rad and the conventional Fastsim contact formulation is used to simulate the wheel/rail contact forces. The contact point search algorithm can manage the multiple contact point condition. Each contact patch is divided into 10 x 20 elements. Each cell can have either the slide or stick condition in each time step of simulation. Figure 23 presents an instance when the wheel profile, (green line) is in contact with the rail profile in both tread and flange regions.

A simplified track stiffness element is defined that also acts as a linear damper under each rail. The stiffnesses under each rail are defined as 44 *kN/mm* and 18 *kN/mm* in the vertical and lateral directions respectively. The corresponding damping is also defined as 400 *kN/(m/s)* and 100 *kN/(m/s)* in the vertical and lateral directions.

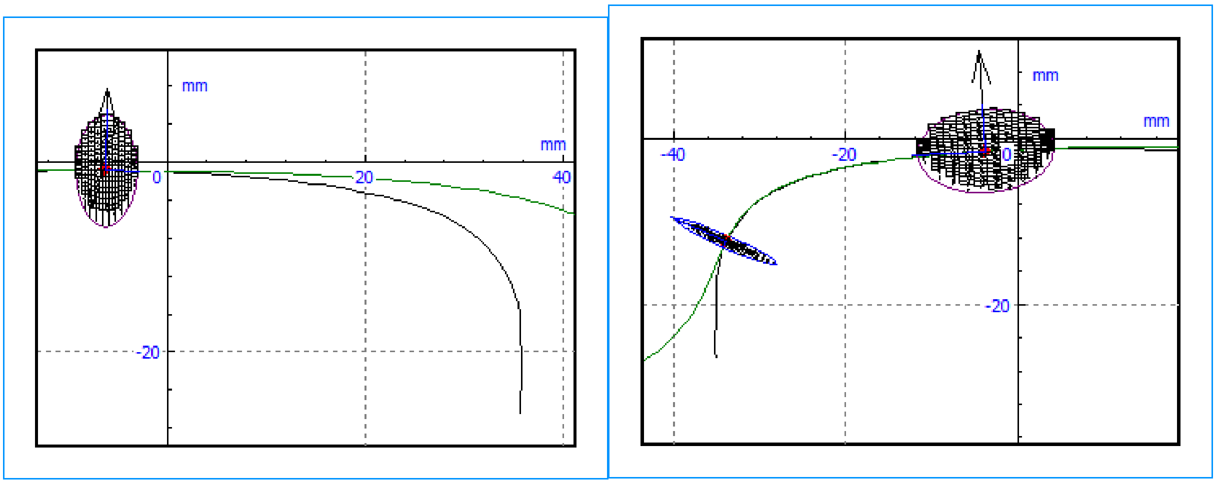

Figure 23: Multiple contact point condition between wheel and rail and slip / stick condition of the contact area cells.

5.3.4. Stability analysis

The critical speed for lateral stability of the system is evaluated as the maximum forward speed of the coach that leads to undamped oscillations of any of the wheelsets or undamped yaw oscillations of the carbody.

A simplified method of stability analysis is initially used to find an approximate maximum speed of the coach. A half sine lateral deviation of track with wavelength of 20 *m* and amplitude of 15 *mm* lateral deviation is defined. Figure 24 shows the angle of attack of different wheelsets of the coach running over the track deviation at speeds of 100 *m/s* and 109 *m/s*. At 100 *m/s* (360 *km/h*) the energy transferred by the lateral disturbance is not enough to disturb the system from its balanced state. By increasing the forward speed to 109 *m/s* (392 *km/h*), the variations of angle of attack of the wheelsets are not damped to zero after passing over the irregularity.

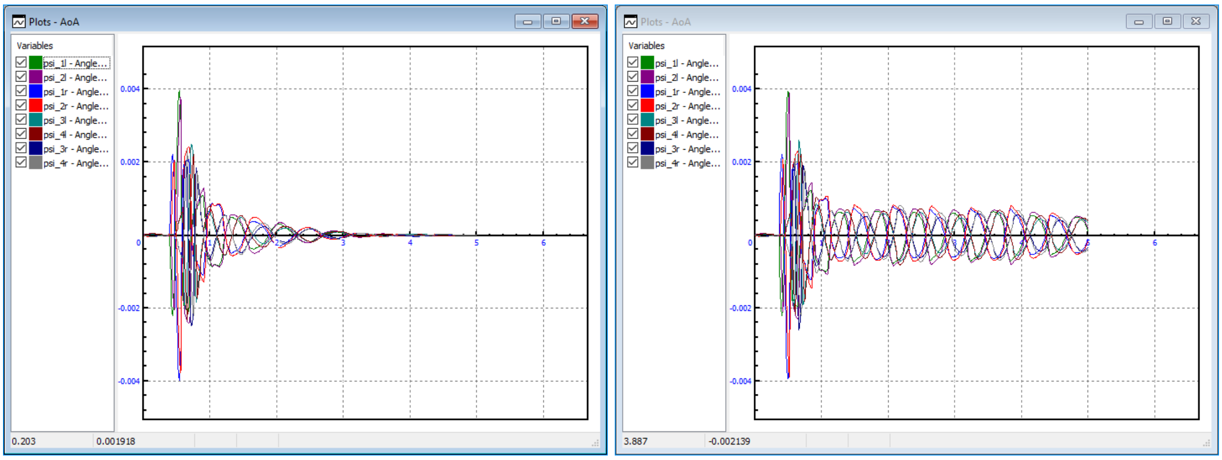

(a) (b)

Figure 24: Variation of angle of attack (psi), for the four wheelsets of the coach, for the left and right wheels, (a) at 100 m/s and (b) at 109 m/s.

6. Results

6.1. Journal Bearings

For each scenario an analysis similar to that shown for the test cycles can be performed. The axial and radial forces acting on the journal bearings are measured virtually during the simulations. To compare the values, the occurring values of the axial forces and the ratio between axial and radial forces are analysed.

The following time-domain results, shown in Figure 25 to Figure 27, were generated with the Simpack model of the ICE-1, adaptation 1 for bearings. In detail, each of the four wheelsets of the vehicle model needs to support a certain amount of axial force. This force is transmitted to the bogie frame and the vehicle body to guide the vehicle through the simulated scenarios. These forces are extracted from the simulation results.

The dynamic behaviour of the vehicle, and therefore also the bearing loads, depends on the forces acting in the wheel-rail contact. The behaviour observed in the defined scenarios may be explained as follows. The radial load acting on the bearing depends on superposed forces: the static gravitational load, the quasi-static load deriving from Unbalanced Lateral Acceleration (ULA), and the dynamic load originating for example from track irregularities. For running speeds higher than the balance speed in curves, at which the lateral component of gravitational forces due to track superelevation exactly compensates the lateral inertial (centrifugal) forces, the bearings on the outer side with respect to the curve will experience a load increase; conversely those on the inner side will see a load decrease.

The axial load acting on a journal bearing is a part of the overall axial load acting on the wheelset through the wheel-rail contact. The other bearing of the same wheelset necessarily supports the remaining part of the overall load. The overall wheelset axial load is basically the difference between the lateral loads acting on the two wheels. These loads also depend fundamentally on the ULA, with increases in this parameter "shifting" the load to the trailing wheelsets of the bogies. The actual load values depend in a complex manner on the contact conditions (wheel and rail profiles, frictional properties such as adhesion coefficient and presence of flange/rail-gauge-corner lubrication) as well as on key bogie geometrical features (most importantly, their wheelbase) and suspension properties (e.g. plan-view primary stiffnesses). Bogie wheelbase, along with primary stiffnesses and longitudinal (frictional) contact forces, will be an essential determinant for the angle of attack of the leading wheelset, whereas the angle of attack of the trailing wheelset will also heavily depend on ULA. The angles of attack determine the tangential frictional forces which are key constituents of the lateral wheel-rail forces and thus the overall wheelset axial forces.

Scenario 1

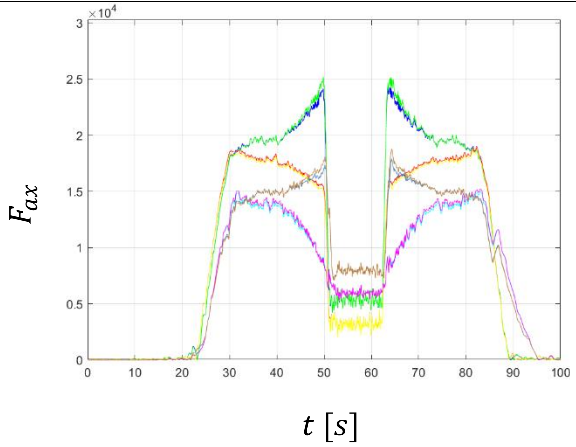

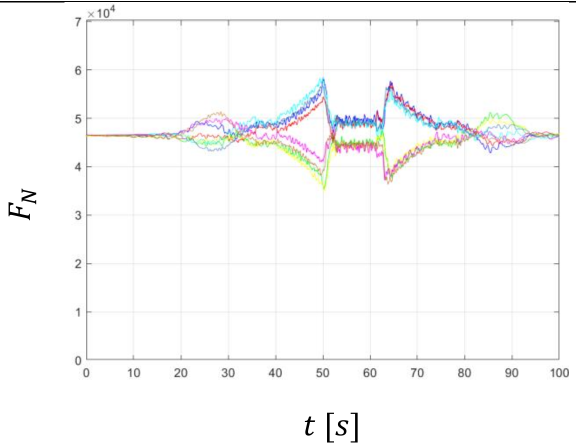

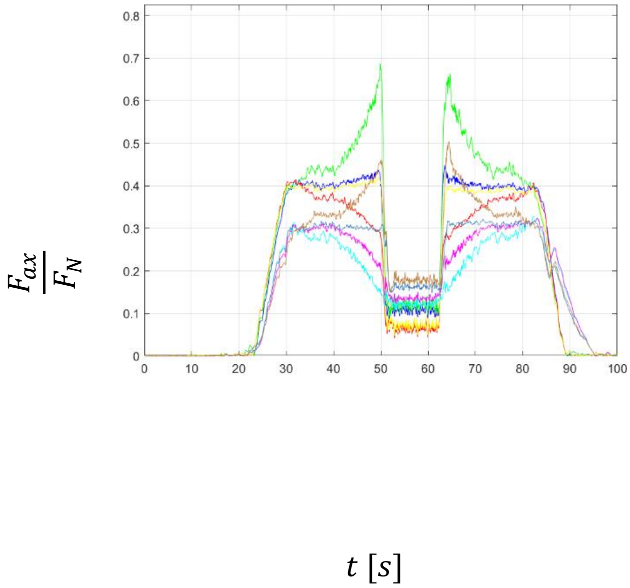

	Bearing 1
	Bearing 2
	Bearing 3
	Bearing 4
	Bearing 5
	Bearing 6
	Bearing 7
	Bearing 8

Figure 25: Forces acting on the bearings in Scenario 1.

Scenario 2

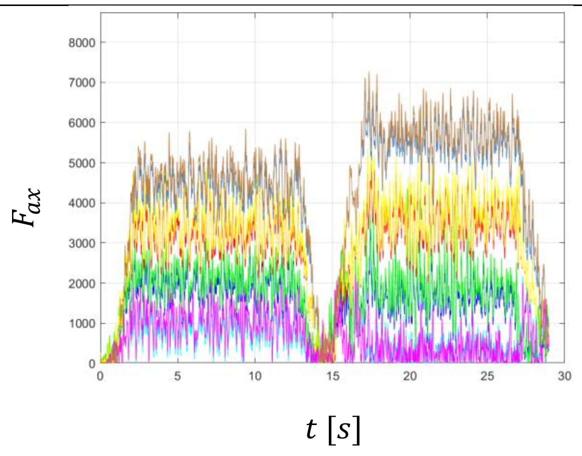

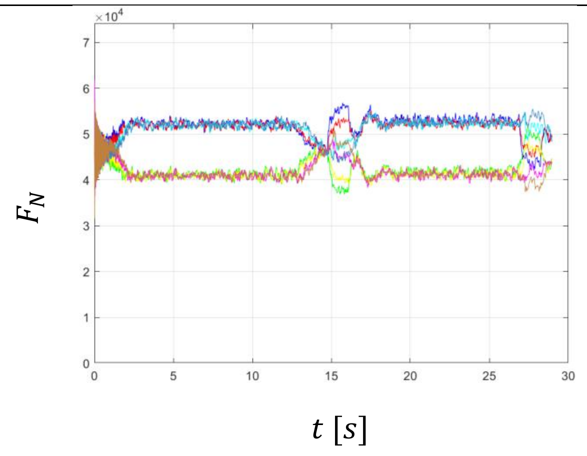

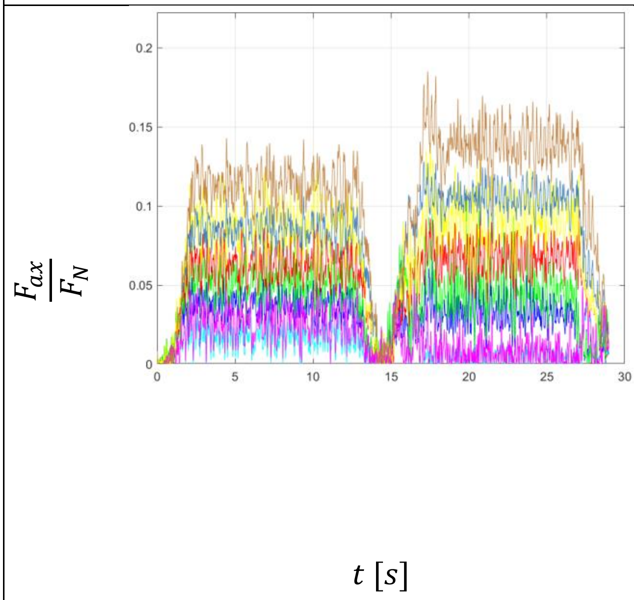

Blue	Bearing 1
Green	Bearing 2
Red	Bearing 3
Yellow	Bearing 4
Cyan	Bearing 5
Magenta	Bearing 6
Steel blue	Bearing 7
Brown	Bearing 8

Figure 26: Forces acting on the bearings in Scenario 2.

Scenario 3

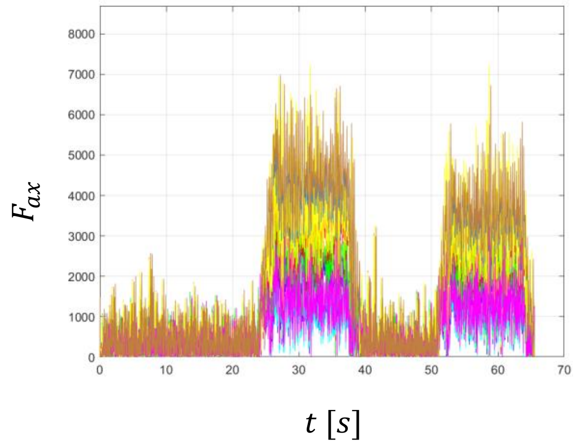

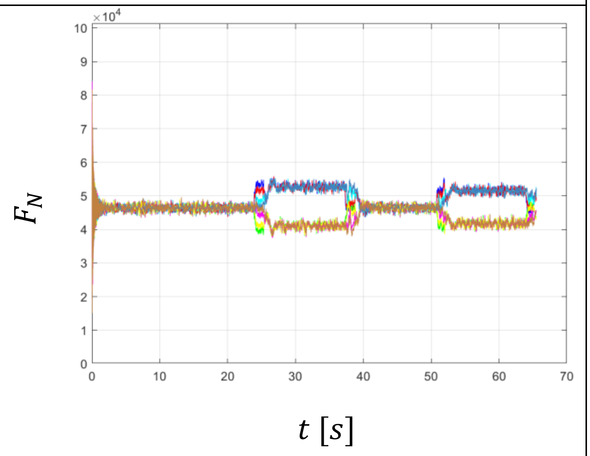

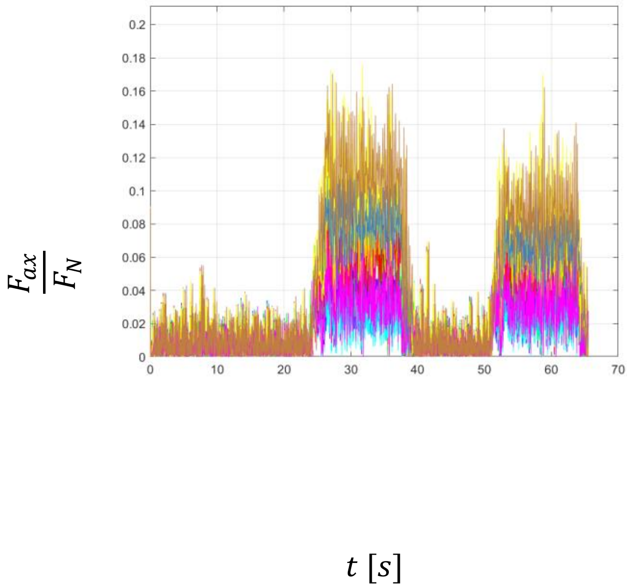

	Bearing 1
	Bearing 2
	Bearing 3
	Bearing 4
	Bearing 5
	Bearing 6
	Bearing 7
	Bearing 8

Figure 27: Forces acting on the bearings in Scenario 3.

A comparison of the axial to radial load ratios, on the one hand those obtained through simulation (peaks of $\frac{\mathrm{F_{ax}}}{\mathrm{F_N}} = 0.65$ on the tightest curves), on the other those used in the EN 12082 test cycle (test value of $\frac{\mathrm{F_{ax}}}{\mathrm{F_N}} = 0.22$ with the formula described in chapter 3.1.1), indicates potentially interesting further work consisting of the analysis of the effects of such differences on bearing lifetime, also considering on the one hand the modelling assumptions affecting the ratio, and on the other hand (probably implicit) safety margins considered in the standard.

6.2. Results for the elastomeric components

The 70 DoF model of the wagon is simulated based on the different scenarios presented in the previous chapters. The forces and moments of the two major elastomeric components are presented in this chapter. Other than presentation the time histories of forces and moments in the different scenarios, the maxima, minima, and averages are presented as a table for each elastomeric component.

As discussed before, the stiffness and damping around the characteristic axis of rotation of the trailing arm bushing is negligible. Therefore, the values of the corresponding bushing moments Mz are not presented (note that in the model the z axis is a lateral axis).

Similarly, the corresponding moments about the z axis of the primary suspension elements are small in the different simulation scenarios. The tighter curves of scenarios 1 and 2 lead to higher lateral and longitudinal forces in the bushings and the other primary suspension elements.

It should be also mentioned that the geometry that represent the elastomeric component of the suspension element is represented as a helical coil. This is just a graphical representation of element.

6.2.1. Response of trailing arm bushings in the different scenarios

The plots in Figure 28 show the time histories of the forces and moments acting on the trailing arm bushings for the front and rear bogies in the three scenarios. The corresponding maxima, minima, and average values are presented in Table 7.

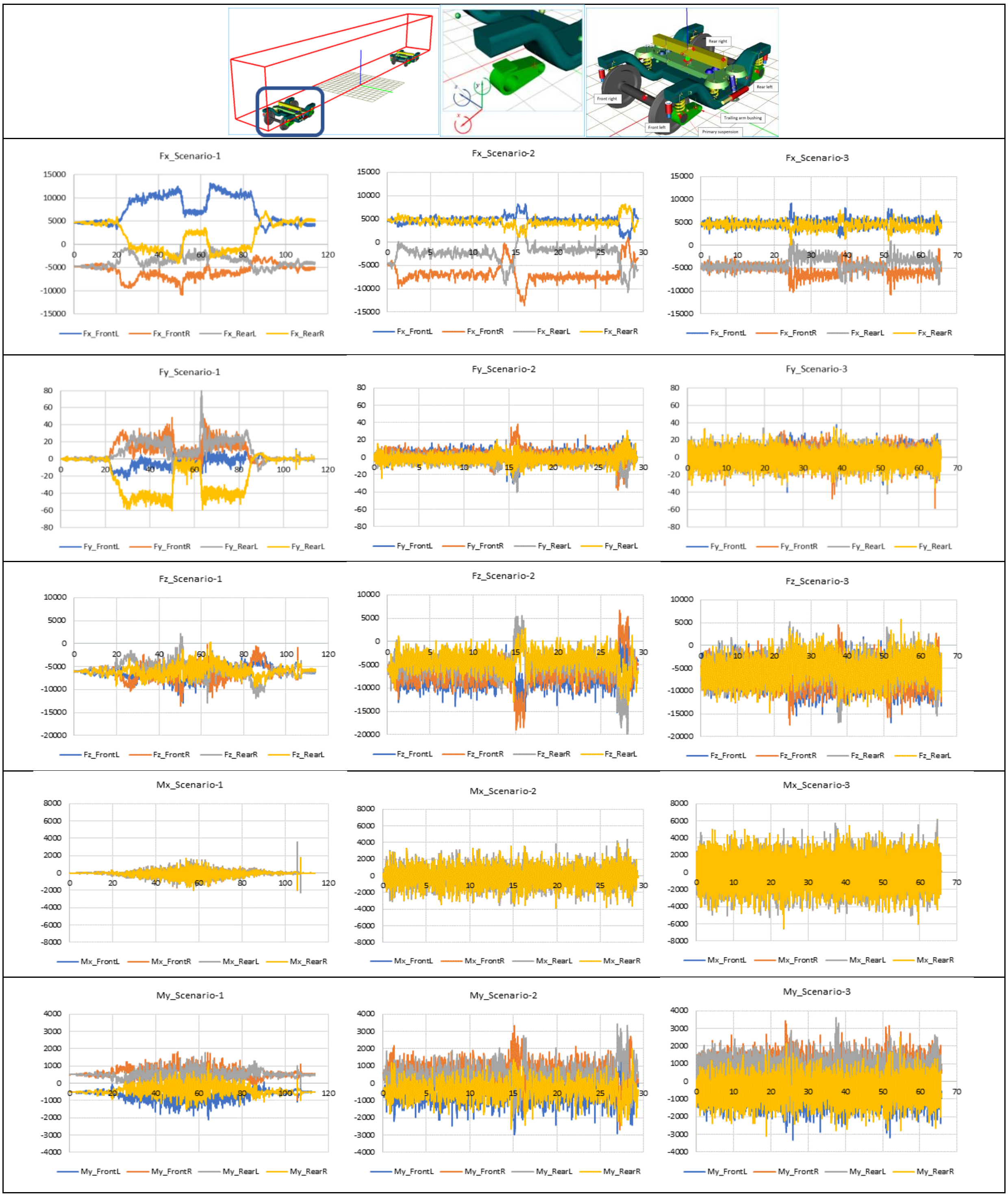

Figure 28: Forces and moments of the bushings of the front bogie of the coach versus time, forces in (N), moments in (N·m) and time in (s).

Table 7 Maximum, minimum and average values of forces and moments in the trailing arm bushing of the front bogie (x: longitudinal, y: vertical, z: lateral axes).

Scenario 1	Fx [N]	Fy [N]	Fz [N]	Mx [Nm]	My [Nm]	Mz [Nm]
Min of mins	-10916	-60	-13500	-2144	-2060	-1
Max of aves	7474	9	-5741	-27	562	0
Max of maxs	13178	80	2222	3534	1804	1
Scenario 2	Fx [N]	Fy [N]	Fz [N]	Mx [Nm]	My [Nm]	Mz [Nm]
Min of mins	-13423	-40	-20260	-3835	-2959	-1
Max of aves	4768	1	-4273	-70	631	0
Max of maxs	8197	38	6620	4333	3412	1
Scenario 3	Fx [N]	Fy [N]	Fz [N]	Mx [Nm]	My [Nm]	Mz [Nm]
Min of mins	-10798	-58	-17316	-6479	-3273	-1
Max of aves	4811	1	-5211	-33	558	0
Max of maxs	9156	38	5731	6151	3618	1

Front Bogie Bushing

	Fx [N]	Fy [N]	Fz [N]	Mx [Nm]	My [Nm]	Mz [Nm]
Min of mins	-13423	-60	-20260	-6479	-3273	-1
Max of aves	7474	9	-4273	-27	631	0
Max of maxs	13178	80	6620	6151	3618	1

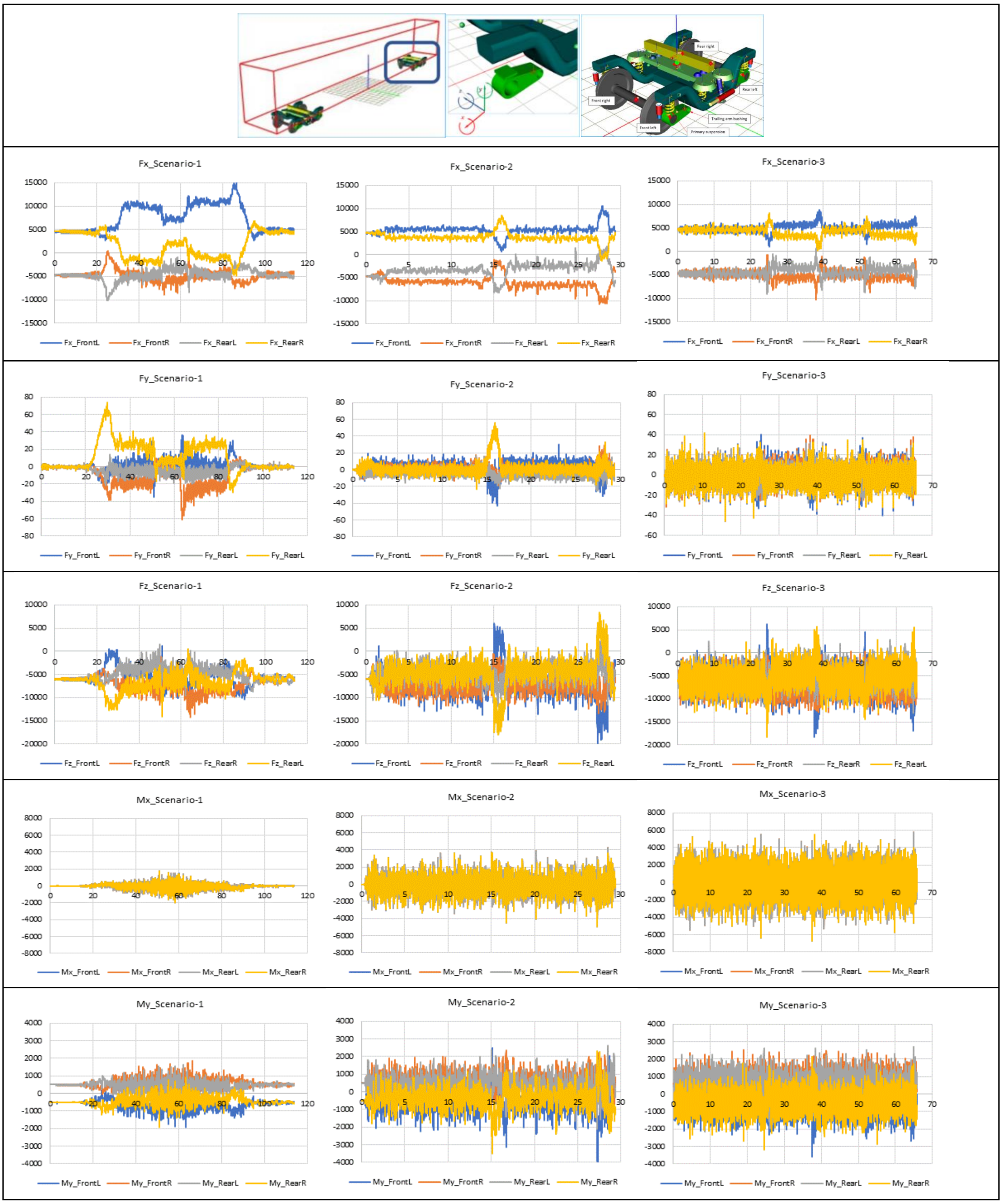

Figure 29: Forces and moments of the different bushings of the rear bogie of the coach versus time, forces in (N), moments in (N·m) and time in (s).

Table 8. Maximum, minimum and average values of forces and moments in the trailing arm bushing of rear bogie.

Scenario 1	Fx [N]	Fy [N]	Fz [N]	Mx [Nm]	My [Nm]	Mz [Nm]
Min of mins	-10100	-60	-14192	-1951	-1885	-1
Max of aves	7489	12	-4981	-27	562	0
Max of maxs	14973	74	1412	1722	1856	1
Scenario 2	**Fx [N]**	**Fy [N]**	**Fz [N]**	**Mx [Nm]**	**My [Nm]**	**Mz [Nm]**
Min of mins	-10572	-43	-19824	-4872	-4079	-1
Max of aves	5374	2	-4592	-66	618	0
Max of maxs	10534	56	8311	4278	2629	1
Scenario 3	**Fx [N]**	**Fy [N]**	**Fz [N]**	**Mx [Nm]**	**My [Nm]**	**Mz [Nm]**
Min of mins	-10139	-45	-18139	-6655	-3570	-1
Max of aves	5044	1	-5308	-33	551	0
Max of maxs	8763	42	6253	5766	2714	1

Rear Bogie_Bushing

	Fx [N]	Fy [N]	Fz [N]	Mx [Nm]	My [Nm]	Mz [Nm]
Min of mins	-10572	-60	-19824	-6655	-4079	-1
Max of Aves	7489	12	-4592	-27	618	0
Max of maxs	14973	74	8311	5766	2714	1

6.2.2. Response of the elastomeric primary suspension in the different scenarios

The plots in Figure 30 show the time histories of the forces and moments acting on the elastomeric spring in front and rear bogies in the three different scenarios. The corresponding maxima, minima, and average values are presented in Table 8.

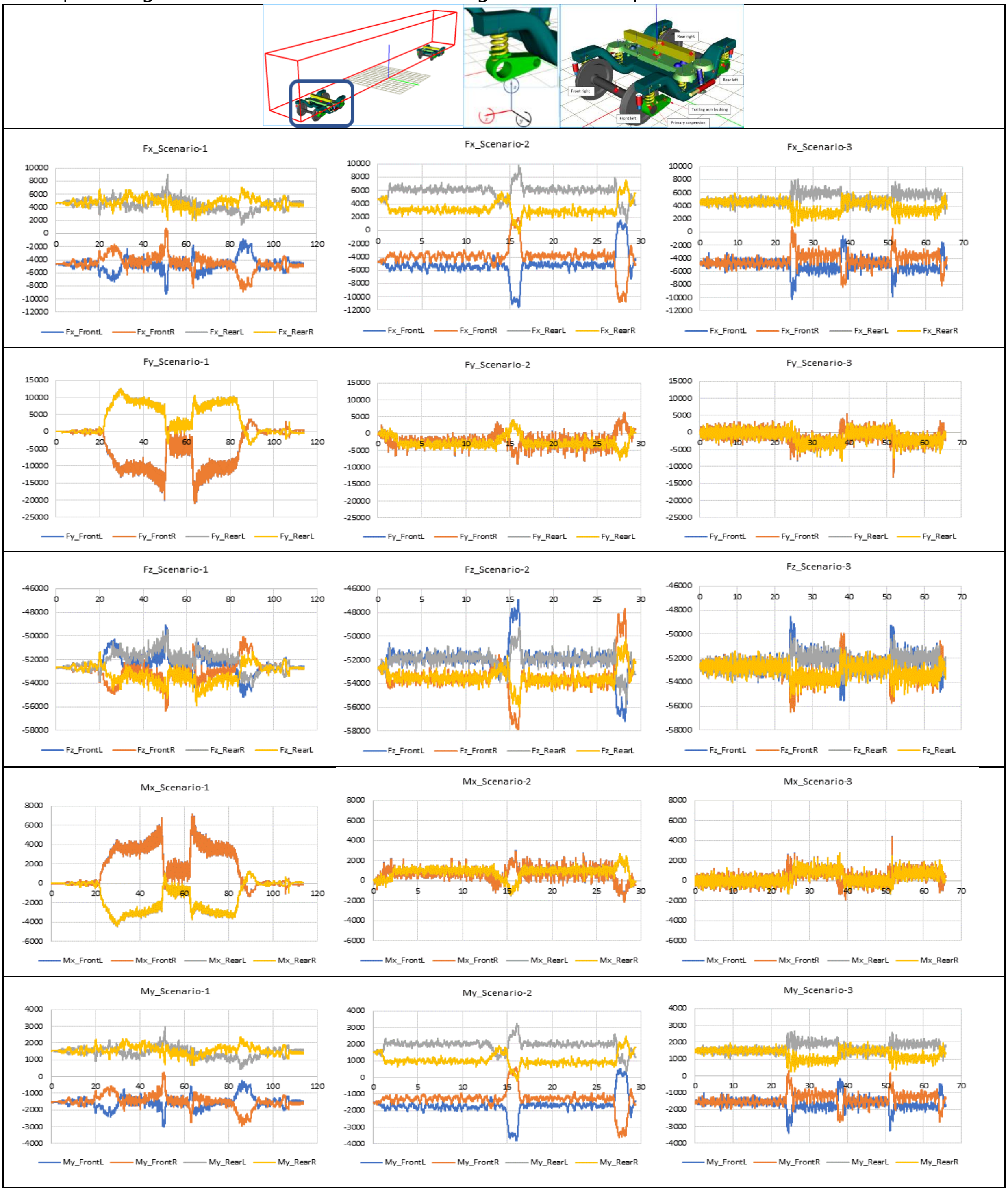

Figure 30: Forces and moments of the primary suspension of the front bogie of the coach versus time, forces in (N), moments in (N·m) and time in (s).

Table 9 Maximum, minimum and average values of forces and moments in the elastomeric primary spring of the front bogie (x: longitudinal, y: vertical, z: lateral axes)

Scenario 1	Fx [N]	Fy [N]	Fz [N]	Mx [Nm]	My [Nm]	Mz [Nm]
Min of mins	-9110	-20790	-56309	-4404	-2991	-45
Max of aves	4793	3807	-52158	1771	1583	-4
Max of maxs	8995	12649	-49045	7181	2964	10
Scenario 2	Fx [N]	Fy [N]	Fz [N]	Mx [Nm]	My [Nm]	Mz [Nm]
Min of mins	-11482	-8951	-57898	-2084	-3790	-20
Max of aves	5910	-2067	-51959	863	1939	3
Max of maxs	9754	6228	-46914	3036	3237	23
Scenario 3	Fx [N]	Fy [N]	Fz [N]	Mx [Nm]	My [Nm]	Mz [Nm]
Min of mins	-10197	-12968	-56472	-1886	-3373	-28
Max of aves	5186	-1064	-52362	371	1694	1
Max of maxs	8066	5522	-48508	4421	2669	14

Front Bogie Primary Suspension

	Fx [N]	Fy [N]	Fz [N]	Mx [Nm]	My [Nm]	Mz [Nm]
Min of mins	-11482	-20790	-57898	-4404	-3790	-45
Max of aves	5910	3807	-51959	1771	1939	3
Max of maxs	9754	12649	-46914	7181	3237	23

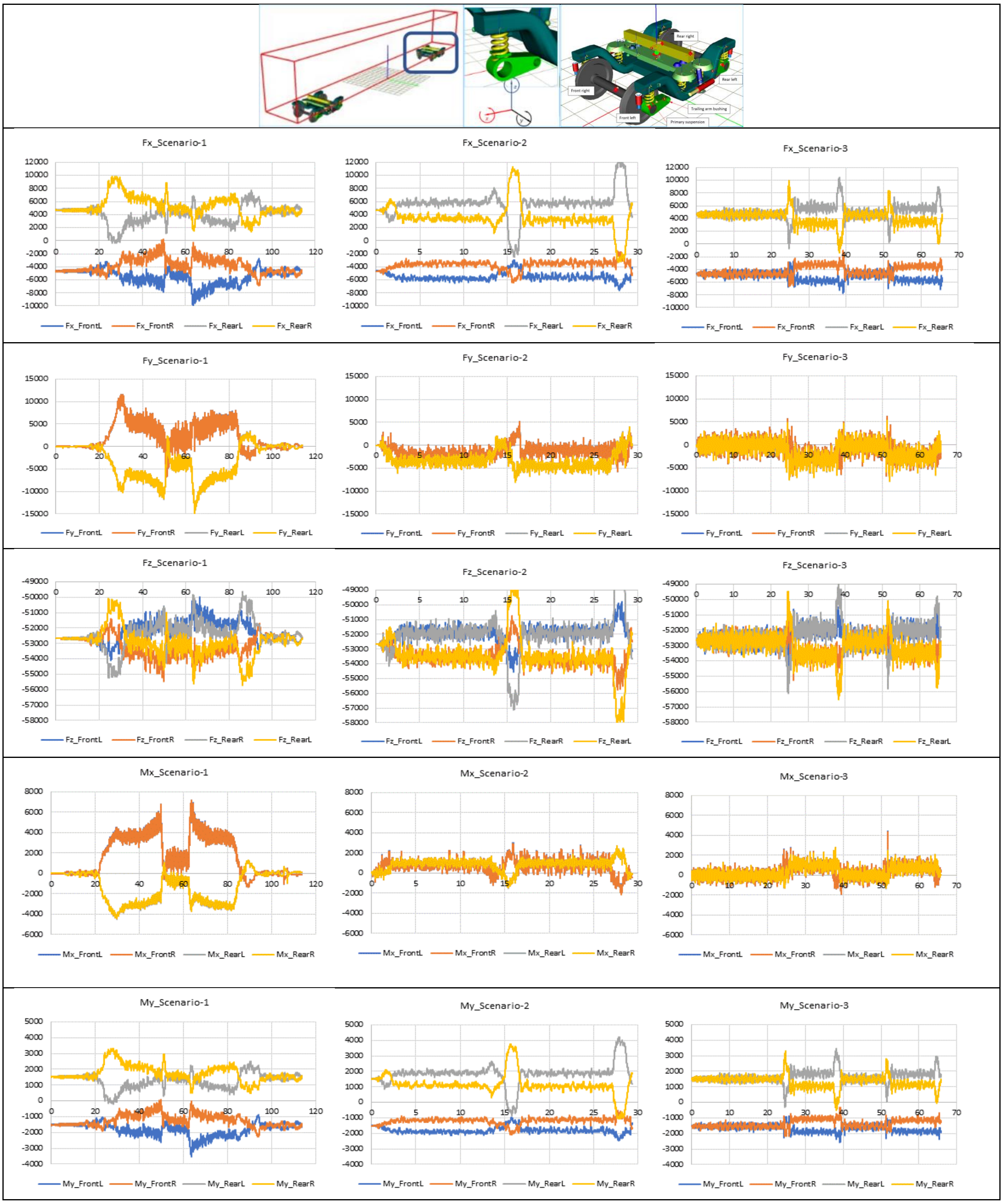

Figure 31: Forces and moments of the primary suspension of the rear bogie of the coach versus time, forces in (N), moments in (N·m) and time in (s).

Table 10 Maximum, minimum and average values of forces and moments in the elastomeric suspension of the rear bogie.

Scenario 1	Fx [N]	Fy [N]	Fz [N]	Mx [Nm]	My [Nm]	Mz [Nm]
Min of mins	-10508	-15017	-55669	-3986	-3513	-16
Max of aves	5283	2208	-52239	1146	1748	7
Max of maxs	9871	11509	-49628	5172	3292	40
Scenario 2	Fx [N]	Fy [N]	Fz [N]	Mx [Nm]	My [Nm]	Mz [Nm]
Min of mins	-7536	-7884	-58178	-1779	-2458	-26
Max of aves	5603	-1346	-51959	1125	1833	5
Max of maxs	12599	5164	-46967	2791	4191	38
Scenario 3	Fx [N]	Fy [N]	Fz [N]	Mx [Nm]	My [Nm]	Mz [Nm]
Min of mins	-7690	-7738	-56505	-2087	-2553	-17
Max of aves	5083	-1020	-52371	398	1658	1
Max of maxs	10432	6070	-48936	2688	3466	23

Rear Bogie Primary Suspension

	Fx [N]	Fy [N]	Fz [N]	Mx [Nm]	My [Nm]	Mz [Nm]
Min of mins	-10508	-15017	-58178	-3986	-3513	-26
Max of aves	5603	2208	-51959	1146	1833	7
Max of maxs	12599	11509	-46967	5172	4191	40

6.2.3. Displacements of the primary suspensions

The displacements of the elastomeric primary suspensions, that represent the linear movements of these elements in the x, y and z directions, are presented Figure 32. In general, the forces and displacements are following the same trends since the stiffness coefficients are constant (linear elastic elements). The variations of displacements are presented around the static point.

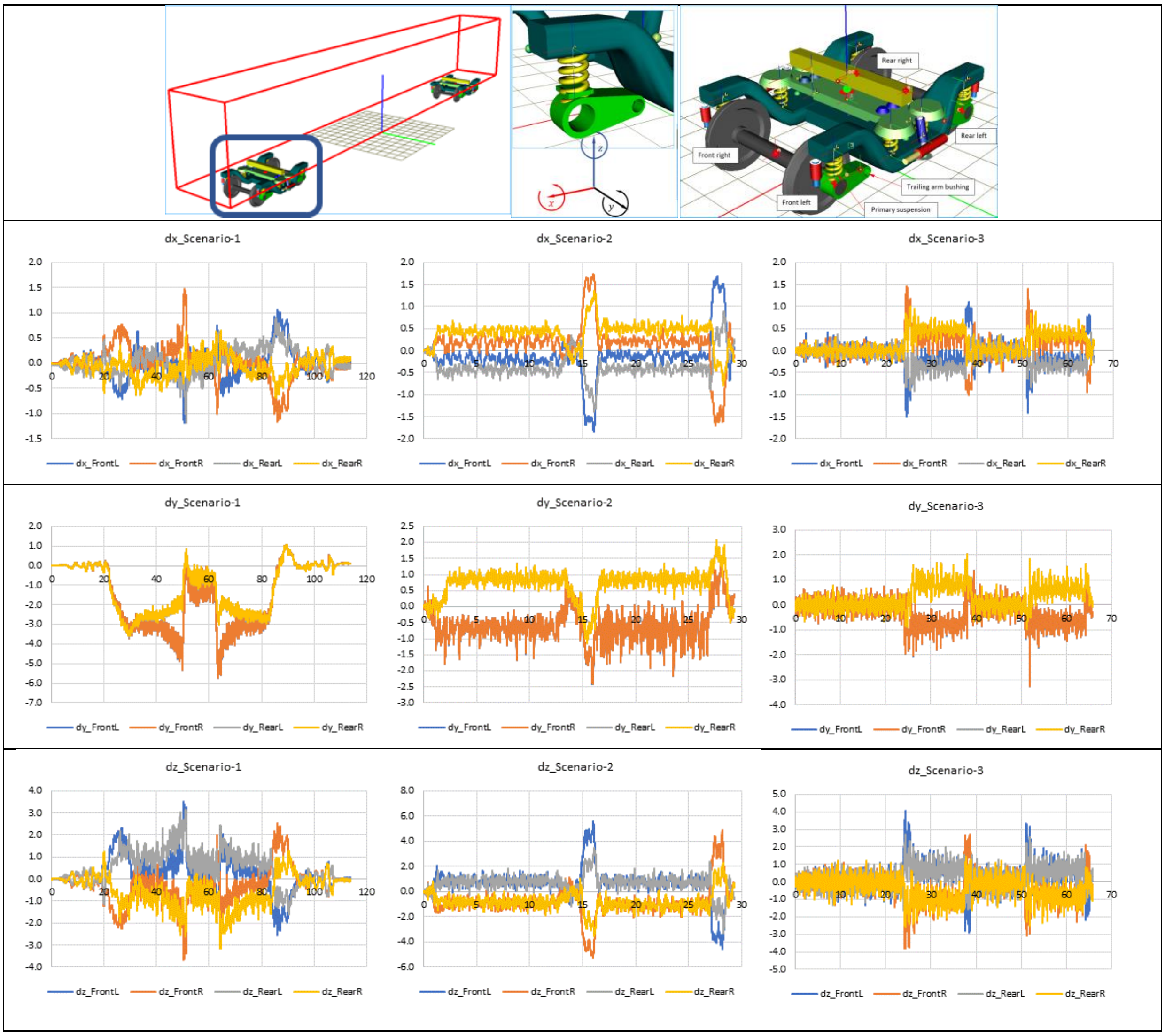

Figure 32: Displacements of the elastomeric primary suspensions of the front bogie of the coach versus time, vertical axis of the graphs are displacements in (mm) and horizontal axis is time in (s).

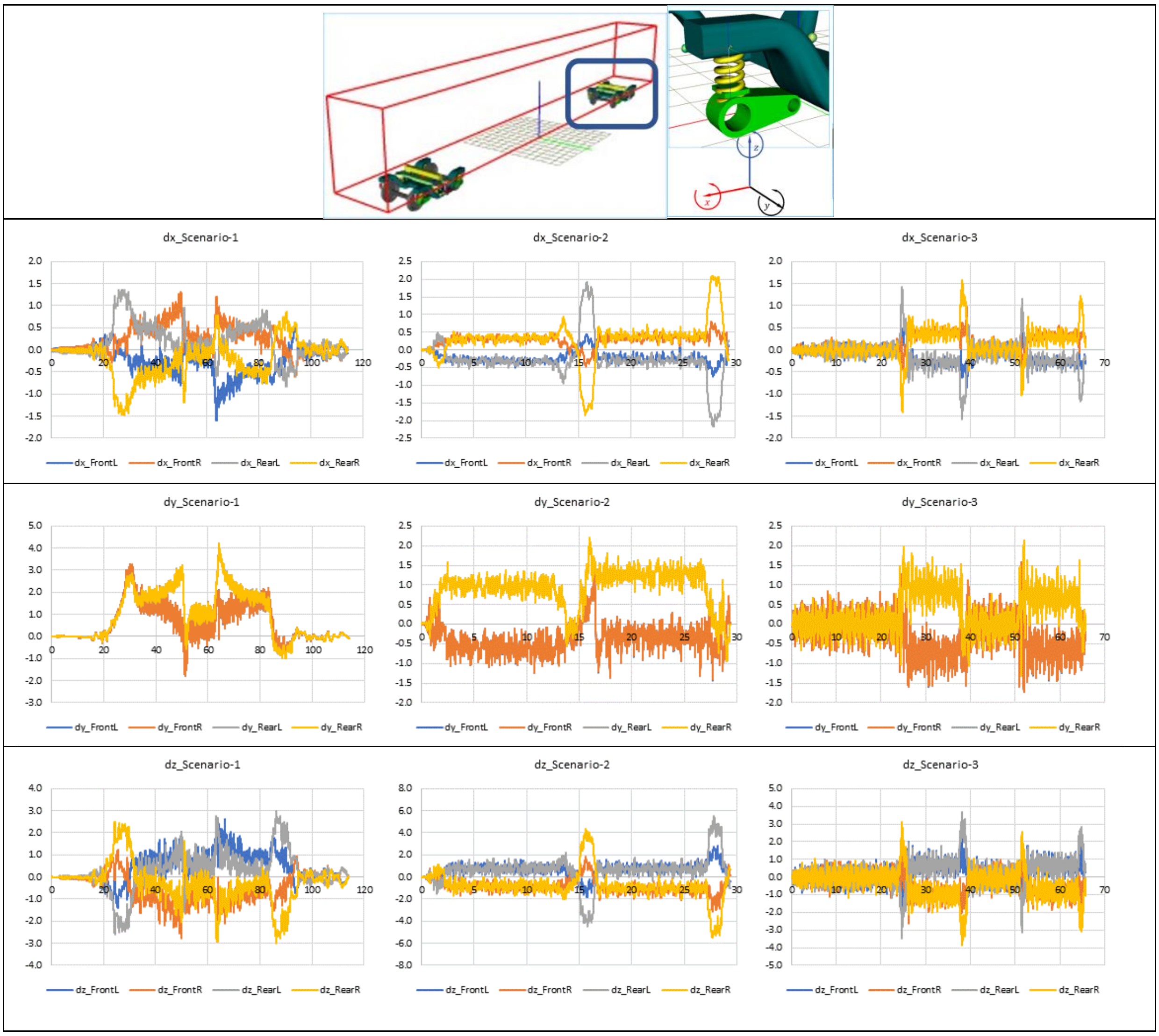

Figure 33: Directional displacements of the elastomeric primary suspension of the rear bogie of the coach versus time, vertical axis of the graphs are displacements in (mm) and horizontal axis is time in (s).

The general geometry of the elastomeric component and its deformation, resulting from the occurring loads in interaction with the stiffness of the elastomeric component are a part of EN 13913 standard. Figure 34 is extracted from the simulations and presents the linear stiffness of the primary suspension in x, y, and z directions. The slope of the graphs has a direct correlation with the defined values in section 5.1. The lack of observed damping effects for *Fz* (lateral) is due to the fact that the damping is simulated only in the vertical direction via the bi-linear damper shown in Figure 20.

The observed static vertical load of approximately 52250 *N* is related to the load in the static condition of the system. The prestress of the primary suspension of 5000 N in the x-direction (longitudinal) is balanced by an equal and opposite force of the bushing in the trailing arm joint. The details behind the pre-stress loads lies within the scope of detailed bogie design and can have a considerable effect on the lifetime of the elastomeric component.

Moreover, it should be highlighted that the initial guess of the vertical stiffness of the primary suspension is deemed to be high, as the system has only 7 mm of deflection in the vertical direction.

Therefore, in the future phases of the project, an improved simulation method of the response of the elastomeric elements will be integrated into the MBS model and a slightly softer spring will be defined.

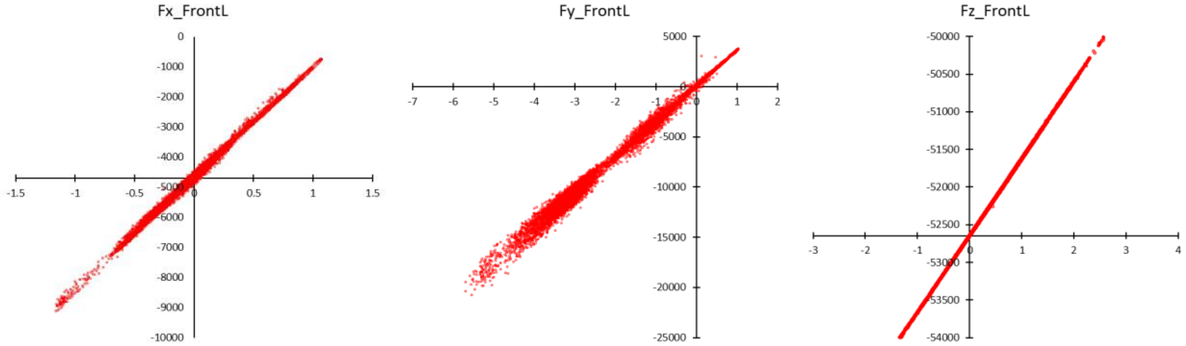

Figure 34: Forces versus displacements of the elastomeric primary spring in x, y, and z.

6.2.4. Spectral analysis of elastomeric components force response.

In addition to the calculated absolute values shown above, the frequencies of the loads play an important role in the test cycle of the elastomeric components in contrast to the test cycle for journal bearings. Therefore, the calculated loads are analysed concerning the occurring frequencies of the forces.

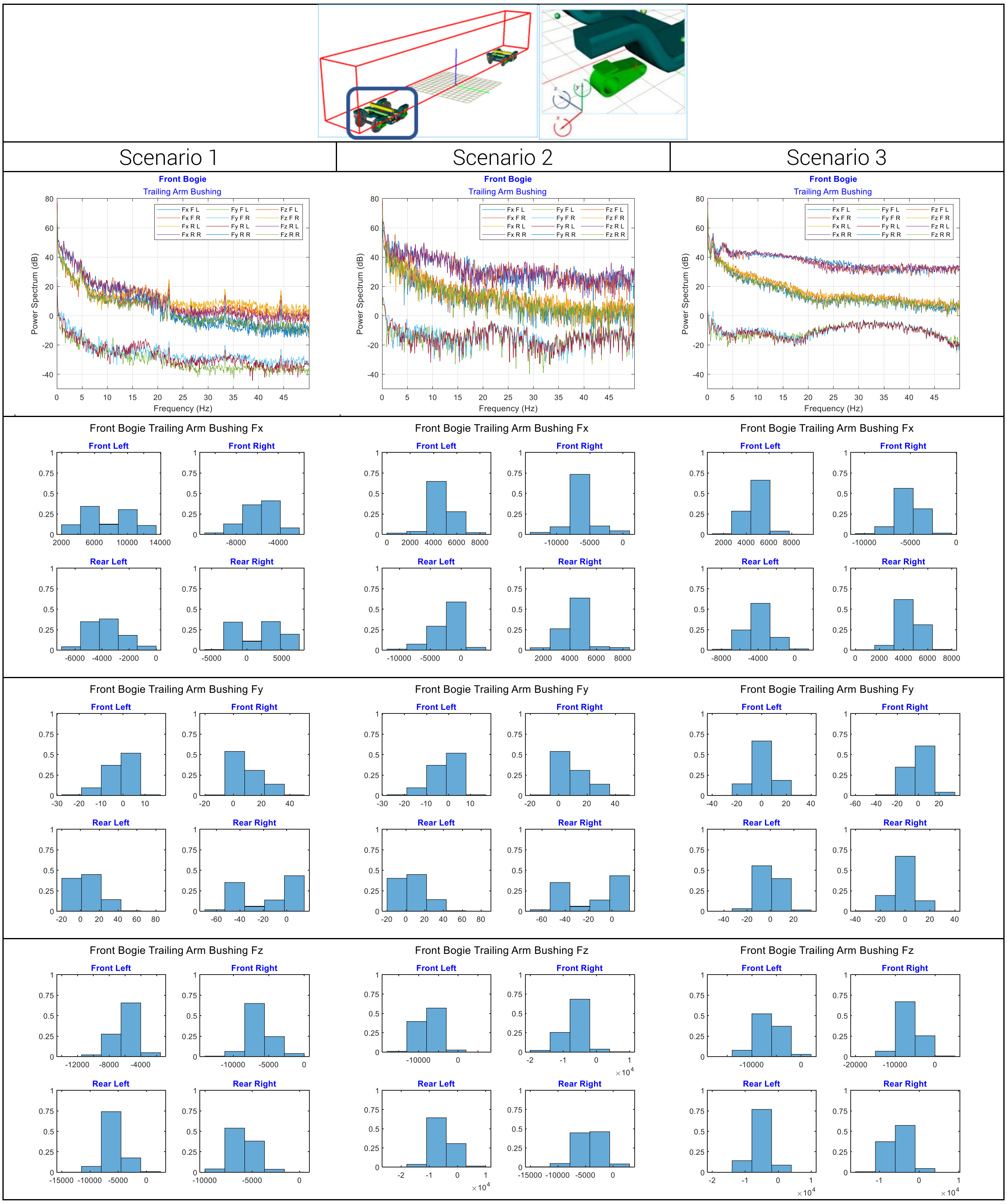

Figure 35: Spectral and histogram representation of the forces in the trailing arm bushing of the front bogie.

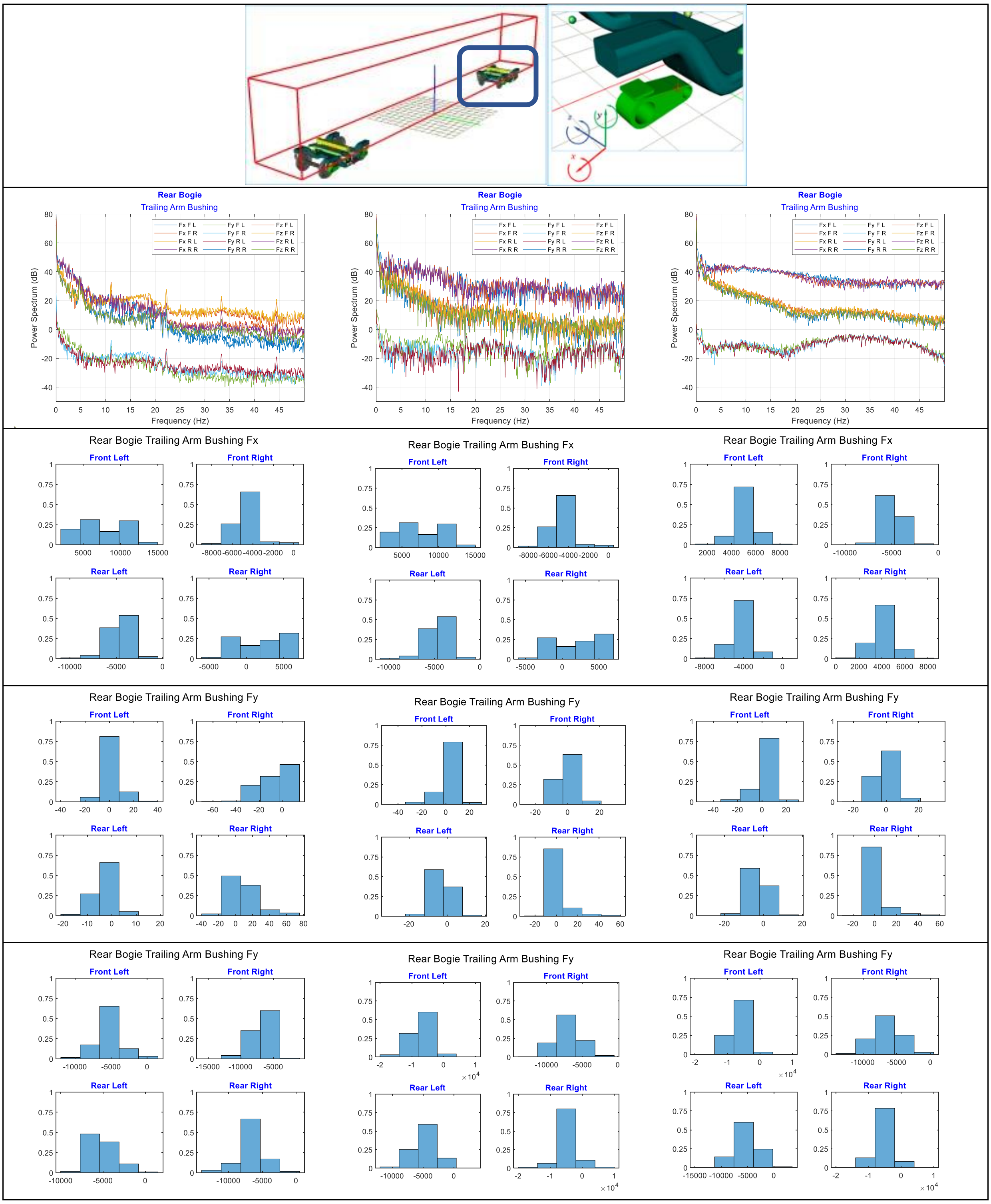

Figure 36: Spectral and histogram representation of forces in the trailing arm bushing of the rear bogie.

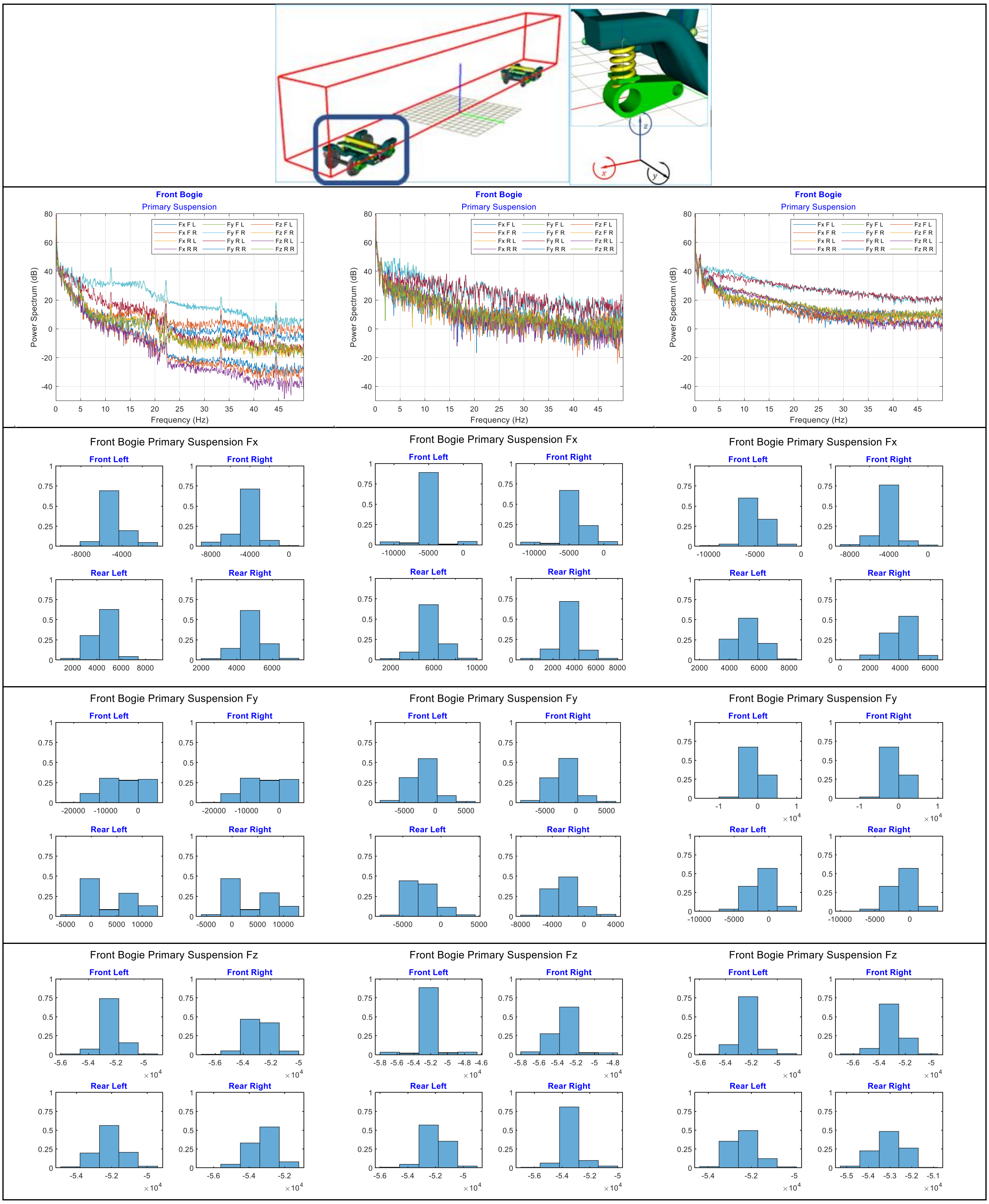

Figure 37: Spectral and histogram representation of the forces in the elastomeric primary spring of the front bogie.

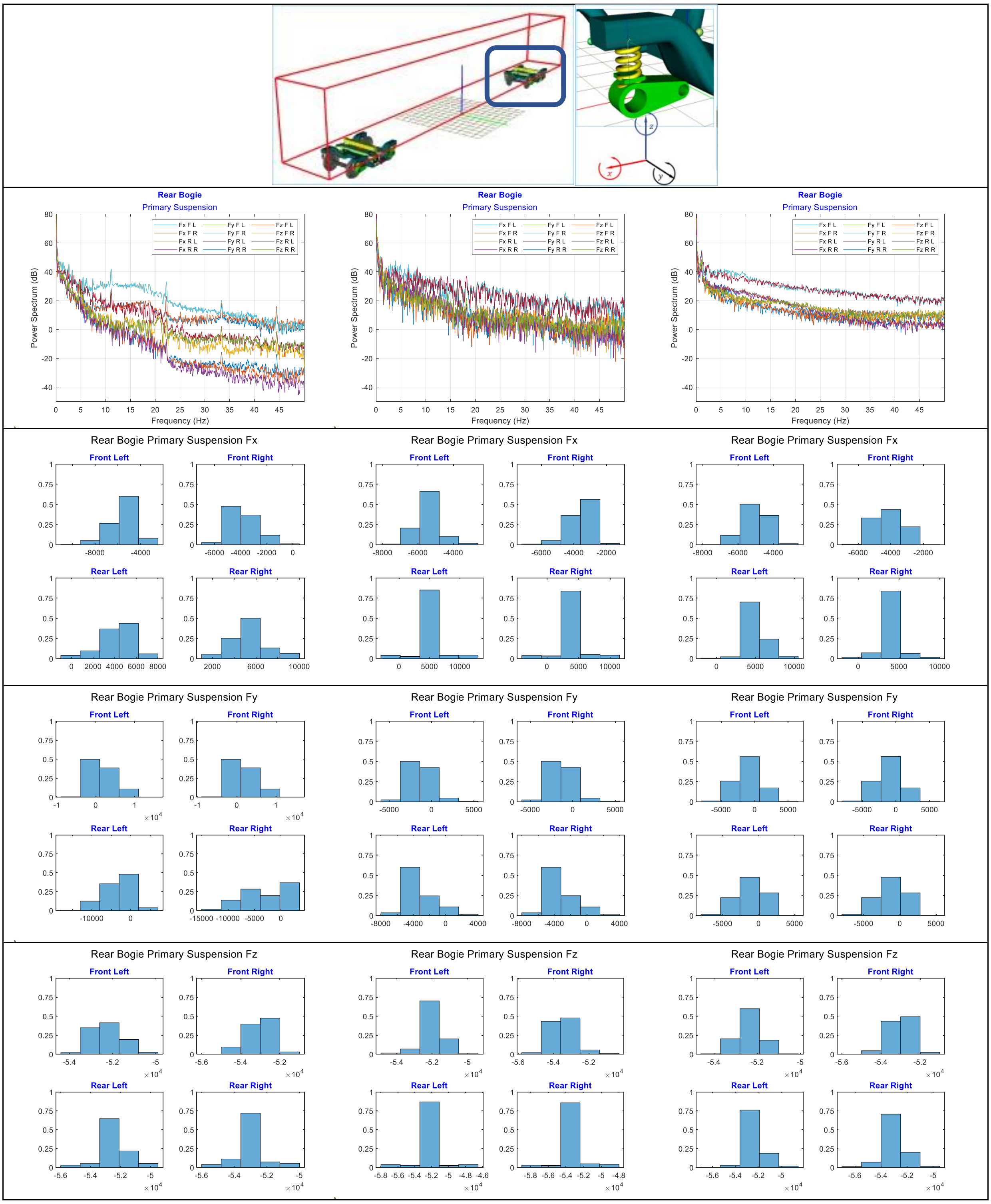

Figure 38: Spectral and histogram representation of the forces in the elastomeric primary spring of the rear bogie.

The objective for presenting the histogram of the loads is to show the range of the loads in limited 5-band ranges. The histogram results will be further used to find the deviation of loads from the nominal design loads of the components.

7. Conclusion

This report describes the investigations on the service loads acting on the components of the type to be developed in GEARBODIES (elastomeric components, journal bearings for railway applications).

As a first step, the EN standards used to assure the proper performance of the components under service loads were analysed. The provisions related to vehicle dynamics were identified along with the quantities that needed to be investigated by simulation due to their relevance for component lifetime.

For this purpose, a set of parameters representing a railway vehicle were chosen. Due to the fact that the availability of public high-speed train models is very limited, a published set of parameters of the German ICE was chosen. Based on this parameter set, two separate MBS models were developed and adapted to simulate the loads acting on the two component types.

For the elastomeric components, an example component for the investigation was chosen. The choice was the bushing connecting the trailing arm of the wheelset to the bogie frame, a design used for highspeed vehicles. This design was implemented and the model shows good dynamic behaviour.

For the investigations of the bearing, the primary suspension was taken as it was given in the base parameters and the secondary suspension was changed. The adaptations performed showed an improvement in the model's original dynamic behaviour but especially in interaction with track irregularities the model does not perform in a manner comparable to a modern high-speed train.

For both investigated components the loads for the test cycle have been determined.

In further work, harmonisation of the models will be pursued by equipping the worse performing model (investigation of bearings with a similar swingarm). At the current state of the investigations, the model is considered as a worst-case scenario for the load investigations on the bearings and the simulations performed might be repeated as soon as the model is adapted.

For both models, three operational scenarios derived from the IMPACT-1 use cases of highspeed trains were developed and used for the simulations. In further work the simulation results will work as a benchmark to evaluate the impact of the components to be developed.

References

Baur, K.(2006). Drehgestelle-(Bogies), EK-Verlage GmbH, Freiburg

Claus, H., Kaiser, I., Küsler, M., Meinders, T., Meinke , P. Reference Data Sets (1997). http://info.itm.uni-stuttgart.de/research/railway/refdataB/ last visit: 19th October 2021

DLR (2018): IMPACT-1: Deliverable D 4.1: Reference Scenario, Shift2Rail, 2018

DIN EN 12082 (2017) Railway applications - Axleboxes - Performance testing

DIN EN 13913 (2003) Railway applications - Rubber suspension components - Elastomer-based mechanical parts

ERRI (1989).: Specification for a Bogie with Improved Curving Characteristics. Bogies with Steered or Steering Wheelsets, ORE (ERRI) B 176, RP1, Vol. 2 (1989). ORE (ERRI), The Netherlands

Hanneforth, W., Fischer, W.(1986). Laufwerke. Transpress Verlag für Verkehrswesen, Berlin